Cables1 links Slit/Robo and Wnt/Frizzled signaling in commissural axon guidance

Zuñiga, Nikole R ; Dumoulin, Alexandre ; Vaccaro, Giuseppe ; Stoeckli, Esther T

DOI: https://doi.org/10.1242/dev.201671

Cables1 links Slit/Robo and Wnt/Frizzled signaling in commissural axon guidance

Nikole R. Zuñiga[1,2], Alexandre Dumoulin[1,2,3], Giuseppe Vaccaro[1,2], and Esther T. Stoeckli[1,2,3,*]

[1]Department of Molecular Life Sciences, University of Zurich, Winterthurerstrasse 190,CH-8057 Zurich, Switzerland
[2]Neuroscience Center Zurich, University of Zurich, Winterthurerstrasse 190,CH-8057 Zurich, Switzerland
[3]University Research Priority Program (URPP) 'Adaptive Brain Circuits in Development and Learning (AdaBD)', University of Zurich, Winterthurerstrasse 190,CH-8057 Zurich, Switzerland

*Corresponding author: E.T. Stoeckli esther.stoeckli@mls.uzh.ch

summary statement: Commissural axons leave the floor plate and turn rostral by a smooth transition from Robo to Wnt signaling. Cables1 links these pathways by transferring Abl kinase from Robo to β-Catenin.

keywords: axon guidance, floor plate, midline crossing, β-Catenin, Wnt signaling, spinal cord development, neural circuit formation

ABSTRACT

During neural circuit formation, axons navigate from one intermediate target to the next, until they reach their final target. At intermediate targets, axons switch from being attracted to being repelled by changing the guidance receptors on the growth cone surface. For smooth navigation of the intermediate target and the continuation of their journey, the switch in receptor expression has to be orchestrated in a precisely timed manner. As an alternative to changes in expression, receptor function could be regulated by phosphorylation of receptors or components of signaling pathways. We identified Cables1 as a linker between floor-plate exit of commissural axons, regulated by Slit/Robo signaling, and the rostral turn of post-crossing axons, regulated by Wnt/Frizzled signaling. Cables1 localizes β-Catenin, phosphorylated at tyrosine 489 by Abelson kinase, to the distal axon, which in turn is necessary for the correct navigation of post-crossing commissural axons in the developing chicken spinal cord.

INTRODUCTION

During the establishment of neural circuits, axons need to connect to distant targets. On their journey, axons are directed by guidance cues provided by cells along their trajectory and from intermediate targets cutting down the long travelling distance into shorter segments. However, navigation of intermediate targets requires precise control of expression and signaling of guidance receptors (De Ramon Francàs et al., 2017; Stoeckli, 2018; Chédotal, 2019; Ducuing et al., 2019). For example, axons of the dI1 subpopulation of commissural axons cross the floor plate, the ventral midline of the spinal cord, without delay. To this end, the attractive response to the intermediate target, the floor plate, has to be turned into a repulsive response upon arrival, in order to prevent lingering of axons in the midline area, but also to prevent axon guidance errors, due to premature expression of guidance receptors sensing repulsive cues, which would prevent axons from entering the midline area.

Commissural axons are entering the floor-plate area due to the interaction between Contactin-2 (aka Axonin-1) on axons and NrCAM on floor-plate cells (Stoeckli and Landmesser, 1995; Stoeckli et al., 1997). Upon contact with the floor plate, commissural growth cones start expressing Robo1 in a Calsyntenin1- and RabGDI-dependent manner (Alther et al., 2016). The temporally regulated trafficking of Robo receptors to the growth cone surface allows detection of the repulsive Slits only upon entry into the floor-plate area, preventing erroneous ipsilateral turns of axons. Expression of Robo1 on the growth cone surface thus expels axons from the floor plate (Philipp et al., 2012; Alther et al., 2016; Pignata et al., 2019).

Post-crossing axons express Hhip receptors, induced by Shh binding to Glypican1 (Wilson and Stoeckli, 2013), to respond to a repulsive gradient of Shh with high levels in the caudal floor-plate area (Bourikas et al., 2005). At the same time, Shh also shapes an attractive Wnt gradient along the anteroposterior axis, with higher Wnt activity levels anteriorly (Domanitskaya et al., 2010; Lyuksyutova et al., 2003). Components of both canonical and non-canonical Wnt signaling have been implicated in dI1 post-crossing commissural axon guidance along the longitudinal axis, suggesting that this strict separation of Wnt signaling into different pathways is not applicable to Wnts' role in axon guidance (Lyuksyutova et al., 2003; Avilés and Stoeckli, 2016; van Amerongen, 2012). More recently, this has been confirmed again by a detailed study of Wnt signaling in midline crossing at the chiasm (Morenilla-Palao et al., 2020).

Despite the fact that midline crossing appears to be a rather simple, binary decision, to cross or not to cross, its regulation has been shown to be extremely complex, involving a large number of guidance cues and receptors. Because the temporal expression of these guidance receptors on

growth cones has to be tightly regulated in order to ensure smooth navigation of an intermediate target, the mechanisms of receptor expression on the growth cone surface have been of great interest. In addition to the subtype-specific response of axons, as shown recently for the ipsi- versus contralaterally projecting retinal ganglion cells (Morenilla-Palao et al., 2020), signaling pathways need to be temporally regulated in the same type of axons. For example, premature expression of receptors for the morphogens presented as gradients along the longitudinal axis of the spinal cord could induce aberrant axonal decisions to turn rostrally along the ipsi- instead of the contralateral floor-plate border.

Our previous studies demonstrated that the responsiveness of only post- but not pre-crossing commissural axons to the antero-posterior Shh gradient is regulated at the transcriptional level: Hhip expression is triggered by Shh binding to Glypican1 on pre-crossing axons (Wilson and Stoeckli, 2013). Similar to the regulation of Robo1 expression, the surface expression of Fzd3, the Wnt receptors on post-crossing commissural axons, is regulated by specific vesicular trafficking (Alther et al., 2016; Onishi and Zou, 2017).

However, we reasoned that exit from the floor plate and turning into the longitudinal axis along the contralateral floor-plate border might be linked by additional mechanisms. A good candidate for such a linker between Slit/Robo signaling and Wnt signaling was Cables1 (Zukerberg et al., 2000; Rhee et al., 2007). In retinal cells, Cables1 was shown to interact with Abl kinase bound to Robo1 triggered by Slit binding, followed by Cables1-mediated transfer of Abl to β-Catenin. This interaction induced dissociation of β-Catenin from N-Cadherin and allowed for phosphorylation of β-Catenin at tyrosine residue 489 by Abl kinase (Rhee et al., 2007).

Here, we show that in the developing spinal cord Cables is required for midline crossing of commissural axons by linking Slit/Robo signaling to Wnt signaling involving phosphorylation of β-Catenin at tyrosine 489 by Abl kinase.

RESULTS

Cables1 is upregulated in dI1 neurons during axonal midline crossing

To study the role of Cables in commissural axon guidance we first examined the expression pattern of *Cables1*. *Cables1* mRNA was ubiquitously detected in the embryonic chicken spinal cord at different stages during commissural axon navigation (Figure 1). The *Cables1* gene produces different proteins due to alternative splicing both in human and chicken (Zhang et al., 2005). The probe we used for in situ hybridization recognizes all isoforms. Using qRT-PCR to distinguish the different

isoforms of Cables1 indicated that isoform X1 is the predominant splice variant in the developing spinal cord (Figure S1A). The dI1 subpopulation of commissural interneurons showed a peak of *Cables1* expression between stages HH22 and HH24, which correspond to critical points in axon navigation, entry and exit of the floor plate, the intermediate target (Figure 1A,B; Movie 1). At HH25, *Cables1* expression in dI1 commissural neurons was reduced to almost the same level that was found throughout the spinal cord (Figures 1B). The ubiquitous expression of Cables in the developing spinal cord was confirmed by immunostaining. At HH23, Cables protein was detected throughout the spinal cord, including the dI1 population of commissural neurons, as confirmed by Lhx2 staining (Figure 1C). Importantly, Cables was also found in axons crossing the midline, stained with Contactin2/ Axonin-1. Because the antibody was raised against a domain of Cables1 that is 90% identical to the corresponding region of Cables2, and therefore does not distinguish between the two proteins, we also studied the expression of *Cables2.* Overall, Cables1 and Cables2 share 55% identity at the protein level. If at all, *Cables2* mRNA was expressed at low levels throughout the neural tube at all stages studied (Figure S1A,B).

Cables1 is required for axons to exit the floor plate and to turn into the longitudinal axis

The transient upregulation of Cables1 in dI1 neurons during axonal midline crossing suggested a role in commissural axon guidance. In order to test for such a role, we performed *in ovo* RNAi at HH17-18 using long dsRNA to downregulate Cables1. We evaluated the efficiency of downregulation by qRT-PCR and observed a 50% reduction for the transcript levels of *Cables1* isoform1 24 hours after electroporation (embryos sacrificed at HH23; Figure S2A). Only 55% of the protein was left when protein levels were analyzed in lysates from embryos sacrificed at HH25 by Western blot (Figure S2B,C). As we successfully electroporated about 50% of the cells in the targeted area with the parameters used in this study, silencing *Cables1* by *in ovo* RNAi almost completely removed protein and transcripts in the electroporated cells.

For the analysis of Cables1 function, we analyzed the trajectory of dI1 commissural axons traced by injections of DiI in open-book preparations of spinal cords dissected at HH25-26 (Figure 2A). Axons in untreated and in GFP-expressing control embryos crossed the floor plate and turned rostrally into the longitudinal axis along the contralateral floor-plate border (Figure 2B). Only 24.3±6.1% and 20.7±7.2%, respectively, of the injection sites showed axons with aberrant navigation. In contrast, when Cables1 was downregulated, axons failed to turn rostrally and stalled in the floor plate, or at the exit site, at 69.8±8.0% of the DiI injection sites (Figure 2B,C,D). These defects were due to the lack of Cables1, because we could rescue axon guidance by co-expressing mouse *Cables1* cDNA

specifically in dI1 neurons using the Math1 enhancer (Figures 2C,D,E). Under these conditions, the percentage of DiI injection sites with aberrant axonal trajectories was strongly reduced (35.25±6.5%). Injection and electroporation of the Math1::mCables1 construct alone (in control embryos) did not have an effect on axon guidance, as aberrant trajectories were seen at only 25.5±4.8% of the DiI injection sites. This is not different from non-treated or GFP-expressing control embryos.

Because we could not fully exclude the possibility that very low levels of *Cables2* were expressed throughout the developing spinal cord, including the dI1 neurons, we also silenced *Cables2*. In contrast to our findings for *Cables1*, silencing *Cables2* did not produce any aberrant phenotypes, suggesting that Cables1 function in commissural axons is specific and cannot be compensated by Cables2 (Figure S3).

To demonstrate that the phenotype seen after perturbation of Cables1 expression was caused by the lack of axonal expulsion from the floor plate and was not due to a decrease in axonal growth speed, we also analyzed axon guidance phenotypes at HH29-30 (Figure S4,A-C). At this stage, axons were still stuck in the floor plate or failed to turn into the longitudinal axis after downregulation of Cables1, indicating that the aberrant phenotype was not simply a delay in normal axon growth. We also ruled out an indirect effect on axon guidance by aberrant neuronal differentiation (Figure S4D).

To provide additional evidence for a role of Cables1 in commissural axon guidance, we used our recently developed *ex vivo* assay to follow commissural axon navigation at the floor plate by live imaging (Dumoulin et al., 2021; Figure 3). To this end, midline crossing by dI1 axons, visualized by Math1::tdTomato-F, was imaged in intact spinal cords embedded in an agarose gel (Figure 3A,B). We did not see any difference in the behavior of pre-crossing axons. Also, the time it took axons to grow from entry to exit point of the floor plate was not different when we compared axons from control-treated and experimental embryos electroporated with dsCables1 (Figure 3B,C). However, in line with the analysis of axonal behavior in open-book preparations of spinal cords from embryos electroporated with dsCables1 (Figure 2B), axons were impaired at the exit site, where we observed failures to turn and aberrant turns into the longitudinal axis (Figure 3B,D,E,F; Movie 2).

Taken together, our results suggest that Cables1 is not required for growth of pre-crossing axons, but that it is important for axons to leave the floor plate and turn into the longitudinal axis.

Cables1 is not required in pre-crossing commissural axons

The absence of an effect of Cables1 on pre-crossing axons was confirmed *in vitro* (Figure 4). We specifically labelled dI1 commissural neurons by electroporation of embryos with a plasmid encoding farnesylated td-Tomato under the control of the Math1 promoter (Figure 4A). When we cultured explants of spinal cords dissected at HH21-22, we found no difference in outgrowth of td-Tomato-positive axons between experimental and control explants (Figure 4B, C).

Cables is required for post-crossing commissural axons' responsiveness to Slit and Wnt5a

Because dI1 commissural axons were found to stall in the floorplate *in vivo* (Figure 2) and to fail to turn at the floorplate exit site *in vivo* (Figure 2) and *ex vivo* (Figure 3), we analyzed their responsiveness to Slit and Wnt5a *in vitro*. When explants were taken from spinal cords dissected at HH26 (Figure 5A), axon lengths were significantly shorter after addition of Slit2 to the medium (compare upper row images of Figure 5B, C, and D; quantified in E). As expected based on previous results (Avilés and Stoeckli, 2016), addition of Wnt5a enhanced axon length by more than 30%. In contrast, no difference in axon lengths were found for explants containing neurons electroporated with dsCables1 (lower rows in Figure 5B,C, and D, quantified in E). The average length did not change in the presence of Slit2 or in the presence of Wnt5a, indicating that Cables1 was required for the responsiveness of post-crossing commissural axons to both Slit and Wnt5a. The average length of axons extending from neurons lacking Cables1 was shorter than the length of control axons.

Cables1 links Slit/Robo1 and Wnt/Fzd signaling *in vivo*

Our *in vitro* results were in agreement with the hypothesis that Cables was required for the responsiveness to Slit and the expulsion of axons from the floor plate, but also for Wnt-dependent turning of post-crossing commissural axons along the contralateral floor-plate border. To test this idea *in vivo*, we analyzed the functional interaction of Cables1 with Robo1 and β-Catenin, respectively. To this end, we used combinations of low doses of dsRNA targeting *Robo1*, *Cables1*, and *β-Catenin* that were not sufficient to induce aberrant phenotypes on their own (Figure 6). We reasoned that if these components interacted together in the same pathway, then combinatorial partial knockdown of these genes would result in aberrant axon navigation. We thus lowered the concentration of the dsRNA used for electroporation that effectively interfered with axon guidance (Figure S5) to levels that were no longer inducing significant changes in axonal behavior on their own (Figure 6B). However, when we combined low concentrations of dsRNA targeting *Cables1* and

Robo1, or *Cables1* and *β-Catenin*, we found significant effects on axon guidance, indicating that these molecules act in the same pathway (Figure 6B). As expected, the combination of dsCables1 with dsRobo1 had a stronger effect on midline crossing, whereas electroporation of dsCables1 together with dsβ-Catenin resulted in a marked increase in DiI injection sites with axons failing to turn into the longitudinal axis at the floor-plate exit site (Figure 6C). The effect of combined downregulation of Robo1 and Cables1 would most likely be higher, if the injection and electroporation of the dsRNAs would have been carried out at E2, as Robo1 surface expression appears to be regulated by trafficking (Alther et al., 2016). However, we wanted to use the same protocol for all groups. Taken together, our *in vivo* results obtained after combined knockdown with low concentrations of target genes confirmed a link between Slit/Robo and Wnt/Fzd signaling mediated by Cables1.

β-Catenin is preferentially phosphorylated in the post-crossing segment of commissural axons

To confirm the role of Cables1 as a linker between Slit/Robo and Wnt/Fzd signaling and to get detailed mechanistic insight, we analyzed the distribution of phosphorylated β-Catenin between pre- and post-crossing segments of commissural axons (Figures S6 and S7). Abl kinase phosphorylates β-Catenin at tyrosine residue 489 (Rhee et al., 2007). Staining with a pY489-specific antibody revealed an accumulation of β-Catenin pY489 in the distal, post-crossing axonal segment both *in vivo* (Figure S6B,E) and *in vitro* (Figure S6C,F).

Based on our results demonstrating that Cables1 had an effect on post- but not pre-crossing axons, we compared the localization of total β-Catenin and β-Catenin pY489 in neurons dissected from HH21 and HH26 embryos (Figures 7 and S7). We found no difference in levels of total β-Catenin between proximal and distal segments of pre-crossing or post-crossing dI1 axons (Figure 7B,C). However, β-Catenin pY489 levels were higher in distal segments of post-crossing axons (Figure 7D,E). No such difference between proximal and distal axonal segments was seen for pre-crossing axons (HH21). In growth cones of post-crossing axons, β-Catenin pY489 was predominantly found in the transition zone to the axon and in the central domain of the growth cone (Figure S8).

Next, we looked at the distribution of β-Catenin pY489 in neurons lacking Cables1 (Figure 8). The observed accumulation of β-Catenin pY489 in the distal axon disappeared in the absence of Cables1, indicating that Cables1 was responsible for the accumulation of β-Catenin pY489 in the distal post-crossing axons.

Phosphorylation of β-Catenin at position Y489 is required for post-crossing axon growth

Next, we wanted to test our model that Cables1-mediated localization of phosphorylated β-Catenin in the distal axon/growth cone was required for axon guidance *in vivo.* To this end, we generated two different β-Catenin mutants: β-CateninY489E, a phosphomimetic (constantly active) mutant, and β-CateninY489F, a mutant that cannot be phosphorylated (non-active form) (Figure 9). Both mutant forms of β-Catenin were specifically expressed in dI1 neurons with the help of the Math1 enhancer (Figure S9). Aberrant axonal turning into the longitudinal axis in the absence of Cables1 was rescued by co-expression of β-CateninY489E, the constantly active form of β-Catenin, but not with the non-active mutant of β-Catenin, β-CateninY489F (Figure 9). The overexpression of each of these mutant versions of β-Catenin, Math1::β-CateninY489E and Math1::β-CateninY489F in the presence of Cables1 did not result in axon guidance phenotypes per se. These results confirm a role of Cables1-mediated activation of β-Catenin, that is phosphorylation of β-Catenin at Y489, in the induction of post-crossing commissural axons' responsiveness to Wnt.

Robo1 is required for the phosphorylation of β-Catenin at Y489

To provide additional evidence for our findings that Cables1 links Slit/Robo1 and Wnt signaling in dI1 axon navigation, we tested the necessity for Robo1 in the phosphorylation of β-Catenin at Y489 (Figure 10). Axons taken from embryos electroporated with dsRobo1 showed lower levels of β-Catenin pY489 (Figure 10A,B). Finally, we further tested the link between Slit/Robo and Wnt signaling by exposing explants of dI1 neurons to Wnt5a (Figure 10C). In contrast to neurons taken from control embryos (see Figure 5D,E), neurons from embryos electroporated with dsRobo1 did not respond to Wnt5a added to the medium (Figure 10C,D).

Taken together, our *in vivo* and *in vitro* data support the model (Figure 11) that Cables1 links Slit/Robo signaling during midline crossing with Wnt/Fzd signaling required for post-crossing axons to turn rostral in response to the Wnt gradient upon floor-plate exit. Cables1 is required for the localization of phosphorylated β-Catenin pY489 in distal axons and growth cones, which in turn is required for correct turning of post-crossing commissural axons along the antero-posterior Wnt gradient.

DISCUSSION

Receptor expression on the growth cone surface has to be precisely controlled for different stages of axonal pathfinding, as different receptors are involved in axonal navigation towards the intermediate target, arrival versus departure without lingering, and continuation of growth towards the next intermediate or the final target. Most studies have concentrated on the regulation of receptor expression for a particular signaling pathway. In contrast, this study describes how two known signaling pathways are connected. Using *in vivo* and *in vitro* assays, we identified a role for Cables1 as a linker between the Slit/Robo-mediated floor-plate exit of dI1 commissural axons and their Wnt/Fzd-mediated turn into the longitudinal axis. Previous studies demonstrated that expression of Robo1, the receptor for the repulsive Slit molecules expressed by the floor plate, is regulated at the post-translational level (Alther et al., 2016; Pignata et al., 2019; Kinoshita-Kawada et al., 2019). This mechanism is in line with descriptions in flies, where Robo expression was shown to depend on trafficking as well (summarized by Gorla and Bashaw, 2020). In vertebrates, miRNA-mediated regulation of translation has been identified as additional regulatory mechanism of Robo surface expression (Yang et al., 2018).

Responsiveness to the guidance cues regulating axon guidance along the longitudinal axis of the spinal cord is controlled by different mechanisms. The expression of Hhip (Hedgehog-interacting protein), the Shh receptor on post-crossing axons, is regulated at the transcriptional level by Shh itself in a Glypican-1-dependent manner (Bourikas et al., 2005; Wilson and Stoeckli, 2013). In contrast, expression of Fzd3, the Wnt receptor on post-crossing axons, is regulated by specific trafficking (Alther et al., 2016; Onishi and Zou, 2017). Robo and Fzd receptors are transported to the growth cone surface in a Calsyntenin1-dependent manner but in different vesicles (Alther et al., 2016). Timing of vesicular transport of Robo1 and its insertion into the growth cone membrane has been shown to depend on RabGDI (Philipp et al., 2012; Alther et al., 2016). The timer for Fzd3 transport and insertion is still elusive, as RabGDI is not involved in Fzd3 expression on the growth cone surface.

Here, we characterized the role of Cables1 in dI1 commissural axon guidance at the floor plate. Our studies demonstrate a novel regulatory mechanism and fine-tuning of the temporal sequence of events. Cables1 acts as a molecular linker between the Slit/Robo and the Wnt/Fzd pathway. Our results demonstrate that Cables1 is required for axon guidance (Figure 2) rather than just axonal growth (Figures 3,4, and Figure S4) or neuronal differentiation (Figure S4), although growth and guidance cannot be separated for post-crossing axons (Figures 2 and 5). Post-crossing axons are shorter *in vitro* and fail to respond to Wnt5a in the absence of Cables1 (Figure 5).

Our results are in line with a model that suggests an association between Abl and Robo1 in axons crossing the midline (Rhee et al., 2007, but see also Bashaw et al., 2000). Upon Slit binding, Robo1 receptors are internalized and the associated Abl molecule is detached from Robo via Cables1. Cables1 brings Abl in close proximity to β-Catenin, which gets phosphorylated at tyrosine residue 489. This phosphorylation changes the interactions of β-Catenin and prepares it for its role in Wnt signaling at the floor-plate exit site.

Our study is the first report on the involvement of a Robo/Cables1/β-Catenin link in commissural axon guidance. So far, Robo-mediated expulsion of axons from the Slit-expressing floor plate has not been functionally linked to guidance cues for the longitudinal axis. We previously demonstrated a role of β-Catenin in Wnt signaling and guidance of post-crossing commissural axons (Avilés and Stoeckli, 2016). Here, we extend these findings and demonstrate that β-Catenin needs to be phosphorylated at tyrosine 489 for its role in post-crossing axon guidance (Figure 9). This finding is intriguing in the context of a recent study about axonal navigation at the chiasm (Morenilla-Palao et al., 2020). The authors found phosphorylation of β-Catenin at tyrosine 654 in ipsilaterally projecting retinal ganglion cell axons. In contrast to Abl-mediated β-Catenin phosphorylation in post-crossing dI1 axons, which is on tyrosine 489, ipsilaterally projecting axons in the visual system are phosphorylated by EphB1. In both cases, crossing the chiasm and crossing the floor plate requires β-Catenin, as silencing β-Catenin resulted in axonal stalling at the midline (Morenilla-Palao et al., 2020; Avilés and Stoeckli, 2016, this study).

Taken together, our *in vivo* and *in vitro* results suggest a model for Cables1 function that connects the Robo1-mediated exit from the floor plate in response to Slit binding to the attractive effect of Wnts directing post-crossing axons rostrally (Figure 11). Cables1 links Robo1-bound Abl kinase to β-Catenin. The accumulation of Abl-dependent phosphorylation of β-Catenin at tyrosine 489 (Y489) in the growth cone/distal axon is required for post-crossing axons to respond to Wnt5a. Our results demonstrate that Cables is required for the distal localization of phosphorylated β-Catenin-pY489 (Figure 8). In turn, co-electroporation of a dominant active form of β-Catenin-pY489, β-Catenin-Y489E, can rescue the lack of Cables1 (Figure 9), indicating that β-Catenin-pY489 is required for Wnt responsiveness of post-crossing axons upon floor-plate exit. In turn, phosphorylation of β-Catenin at Y489 requires Robo signaling (Figure 10). Taken together, our experiments suggest Cables1 as a linker between Robo/Slit and Wnt signaling to ensure smooth navigation of commissural axons out of the floor plate and rostral along the contralateral floor-plate border.

EXPERIMENTAL PROCEDURES

Animals

Fertilized chicken (Gallus gallus) eggs were obtained from a local supplier and incubated at 39°C. All the experiments including chicken embryos were carried out in accordance with Swiss law on animal experimentation and approved by the cantonal veterinary office of Zurich.

Method details

In ovo electroporation

After 2 or 3 days of incubation at 39°C, fertilized eggs were windowed for injection and electroporation, as described previously (Wilson and Stoeckli, 2011, and 2012). Embryos were staged according to Hamburger and Hamilton (1992). Unilateral electroporations were performed at embryonic day 3, HH17-18, using 5 pulses of 25 Volts of 50 msec duration and 1 sec interpulse interval.

Plasmids and dsRNA

For functional gene analysis, chicken embryos were injected and electroporated with long dsRNA (300 ng/µl) derived from the target gene (500 ng/µl for dsCables1) and a plasmid encoding β-actin-driven hrGFP (25 ng/µl). For hypomorphic experiments, combination of low doses (75 ng/µl) of each dsRNA were used (see Supplementary Table 1 for details).

For the pY489 phospho-mutant versions of β-Catenin, we used the Q5 Site-directed mutagenesis kit (NEB) to generate β-CateninY489F, a form of β-Catenin that cannot be phosphorylated at tyrosine 489 due to the exchange of tyrosine 489 with phenylalanine, and β-CateninY489E (exchange of tyrosine 489 with glutamic acid), a phosphomimetic form of β-Catenin that is dominant active. The following primers were used for the phosphomimetic substitution of Tyr (tat) by Glu (gaa): Fw: 5'-TCGCCTTCATcaaGGACTGGCCTGTTG-3' Rv: 5'-ACGGCATTCTGGGCCATC-3'. For the phosphoinhibited substitution of Tyr (tat) by Phe (ttt): Fw: 5'-TCGCCTTCATtttGGACTGCCTG-3' Rv: 5'-ACGGCATTCTGGGCCATC-3'. For rescue experiments, the ORF of mouse Cables1 was obtained from Biocat/Origene. The amplified PCR fragment was subcloned via HIFI cloning (NEB) under a Math1 enhancer.

Open-book preparations and DiI tracing

Spinal cords were dissected at HH25-26 (E5) as open-book preparations and fixed for 30 min in 4% PFA in PBS. To label dI1 commissural neurons, we injected Fast-DiI (5 mg/ml in ethanol; Thermo Fisher) into the area of the cell bodies in the dorsal spinal cord, as described previously (Wilson and Stoeckli, 2012; Perrin and Stoeckli, 2000). The trajectory of dI1 axons at each DiI injection site was analyzed by a person blind to the experimental condition and categorized as 'normal', 'floor-plate stalling', or 'no turns'. A 'normal' phenotype consists of axons entering and crossing the floor plate with an exclusively rostral turn into the longitudinal axis of the spinal cord at the floor-plate exit site. When at least 50% of the DiI-labelled axons failed to reach the contralateral floor-plate border, the DiI-injection site was counted as 'floor-plate stalling'. When >50% of the axons reaching the exit site failed to turn rostral, the DiI injection site was classified as showing a 'no turn' phenotype. If less than 10 axons reached the floor-plate exit site, we did not assess the turning phenotype at this site. For quantification, we calculated the ratio of DiI injection sites per embryo with either a normal, a 'floor-plate stalling' or a 'no turn' phenotype. However, for statistical analyses between different experimental groups, we combined the different aberrant phenotypes into one group, as the two phenotypes ('floor-plate stalling' and 'no turns') are not independent of each other. At a DiI injection site where all or almost all axons fail to reach the floor-plate exit site, a failure to turn cannot be assessed. Therefore, in our analysis of dI1 trajectories, the number of DiI injection sites with aberrant turning in experimental groups are likely to be underestimated. We would also like to stress that our quantification is independent of the actual number of axons labelled by the injection of DiI. It was always very easy to assess whether the majority of the axons crossed and turned, and it was always the same person analyzing the trajectories of dI1 axons.

For embryos dissected at HH29-30 (E6), ipsilateral turns or ipsilateral stalling was observed, but excluded from the quantification, as later developing populations of axons labelled by late DiI injections normally extend to the floor plate without crossing. Therefore, these normally navigating axons could not be distinguished from dI1 axons stalling at the floor-plate entry site. Images were acquired using an Olympus BX61 microscope equipped with a spinning disk unit. Data are given as mean±sem (standard error of the mean). Statistical analysis was performed using Prism 8 (GraphPad).

In situ hybridization and immunostaining

Embryos were sacrificed and fixed in 4% paraformaldehyde in PBS at room temperature for different times depending on the stage. The tissue was cryoprotected by incubation in 25% sucrose/PBS and then embedded in Tissue-Tek O.C.T Compound (Sakura). Specimens were frozen in isopentane on dry ice and stored at −20°C. Sections of 25 µm thickness were obtained using a cryostat (LEICA CM1850). Expressed sequence tags (ChESTs; SourceBioScience, Table 1) were used to generate *in situ* probes using a DIG RNA labeling kit (Roche). In situ hybridization was performed as described (Mauti et al., 2006). Immunostaining was performed as described previously (Perrin et al., 2001; Wilson and Stoeckli, 2011). The complete list of ChESTs and antibodies can be found in Table 1.

For immunostaining, cultures of dissociated neurons and explants were fixed in 4% PFA for 15 minutes at room temperature. Cells and explants were incubated in 100 mM glycine for 20 minutes and permeabilized with PBST (0.25% Triton X-100 in PBS) for 15 min. To reduce unspecific binding of antibodies, cells/explants were incubated in 10% FCS in PBST at room temperature for 30 min. Primary antibodies diluted in 10% FCS/PBST were incubated at 4°C overnight. The following day, cultures were washed twice in PBST and incubated with secondary antibodies diluted in 10% FCS/PBST for 2 hours at room temperature. Before mounting in Mowiol-DABCO, samples were washed three times in PBS.

Quantitative Real-Time-PCR

RNA was isolated from spinal cords of embryos at HH22 and HH25 using the RNeasy mini kit (#74134, QIAGEN). For the evaluation of RNAi efficiency, chicken embryos were electroporated at HH17-18 and neural tubes were dissected 24 hours later under a fluorescence microscope (Olympus SZX12). Total RNA was then reverse transcribed using SuperScript™ III First-Strand Synthesis SuperMix (#18080-400, Thermo Fisher). The primers used for the quantitative Real-Time PCR reaction are listed in Supplementary Table 1. qRT-PCR was performed using the Fast Sybr Green Master Mix (#4385610, Thermo Fisher) and run on a QuantStudio 3 Real Time PCR System (Applied Biosystems). mRNA expression levels were normalized to the expression level of chicken 18S ribosome (Himmels et al., 2017) and quantified using the $2^{-\Delta\Delta Ct}$ method. PCR amplifications were assessed from pools of spinal cords from at least three independent experiments. For quantification of *Cables1* isoform levels and *Cables2*, values were normalized to HH22 *Cables1_X1*.

SDS-PAGE and Western Blotting

For the evaluation of RNAi efficiency, chicken embryos were electroporated at HH17-18 with a combination of two different dsRNAs targeting Cables1 (500 ng/µl each). Neural tubes were dissected 48 hours later under a fluorescence microscope (Olympus SZX12). Cells were lysed with RIPA buffer (150 mM NaCl, 1% Nonidet P-40, 0.5% Sodium deoxycholate, 0.1% SDS, 50 mM Tris-HCl, pH 7.4) supplemented with protease inhibitors (Roche 11836170001) and phosphatase inhibitors (5 mM NaF, 1 mM Na_3VO_4, 10 mM β-Glycerophosphate). Protein concentrations were measured and samples were prepared for PAGE by adding 0.2 volumes of 5X Loading Buffer (650 mM Tris-Cl, pH 6.8, 5 % SDS, 25 % Glycerol, 500 mM DTT and bromophenol blue) and incubated for 5 min at 95°C. Protein samples were separated by SDS-PAGE and transferred to a PVDF membrane. The membranes were blocked with 5% milk in TBST (0.01 M Tris-HCl, pH 7.5, 150 mM NaCl, 0.1% Tween20), followed by primary antibody incubation overnight at 4°C. On the following day, membranes were washed in TBST three times for 15 min, before incubation for 2 h at room temperature with the corresponding secondary antibodies conjugated to horseradish peroxidase. Membranes were washed in TBST before using the ECL Western Blotting Detection Reagent (GE Healthcare). The chemiluminescence signal was detected using the Amersham Imager 600 (GE Healthcare).

Quantification of axonal outgrowth from commissural explants

For average length measurements, only td-Tomato-F-positive dI1 axons (labelled by electroporation of embryos with Math1::td-TomatoF) were used. Each explant was divided into 4 quadrants and the average neurite length from the explant border was measured for each quadrant with ImageJ (v 1.52i, Java 1.8.0_101 64-bit, NIH). Axons were manually traced using a Wacom DTU-1931 tablet and pen tool. Data from at least three different, independent experiments were pooled and normalized to control conditions of each independent experiment. Data are given as mean±sem. Statistical analysis was performed using Prism 8 (GraphPad).

Quantitative Analysis of phospho-Y489 levels in commissural neurons

To analyze total β-Catenin and β-Catenin-pY489 levels in commissural neurons, we performed fluorescence intensity measurements with ImageJ (v 1.52i, Java 1.8.0_101 64-bit, NIH). Axons were carefully delineated (excluding the growth cone) to acquire mean levels of fluorescence. For comparison of axonal distribution, we measured the mean fluorescence in a determined area in the

distal and proximal axon and normalized to total axon levels. To account for background signal, we measured the mean fluorescence value by selecting an area adjacent to the axon. For quantification, at least 20 neurons per condition were measured using a Wacom DTU-1931 tablet and pen tool. Data from at least three different, independent experiments are pooled and normalized to control conditions of each independent experiment. Data are given as mean±sem. Statistical analysis was performed using Prism 8 (GraphPad).

Primary Neuron Cultures and Explant Cultures

Explants of commissural neurons were obtained from dorsal spinal cords dissected from HH25-26 embryos for post-crossing, and HH21-22 for pre-crossing neurons. To ensure that we dissected dI1 commissural neurons, embryos were dissected under a fluorescent stereoscope in order to visualize Math1::td-TomatoF-positive cells. Commissural explants were grown on 8-well LabTek slides (Nunc) coated with poly-Lysine (20 µg/ml; Sigma) and Laminin (10 µg/ml). The medium for commissural neurons was as previously described (Niederkofler et al., 2010), except for pre-crossing cultures, where the medium was supplemented with recombinant Netrin (100 ng/ml, R&D Systems).

For experiments assessing Slit and Wnt responsiveness, control medium or medium containing Slit2 (200 ng/ml; R&D Systems) or Wnt5a (200 ng/ml; R&D Systems) was added to the commissural neurons after 48 hours or to the explants after 24 hours *in vitro*. Explants were grown for additional 20 hours before fixation and immunostaining.

For cultures of dissociated commissural neurons, neurons were obtained from dorsal spinal cords dissected from HH25-26 embryos for post-crossing, and HH21 for pre-crossing cultures. Commissural neurons were grown on 8-well LabTek slides (Nunc) coated with poly-L-Lysine (20 µg/ml; Sigma) and Laminin (10 µg/ml). The culture medium was as previously described (Niederkofler et al., 2010), except for pre-crossing cultures where the medium was supplemented with recombinant Netrin (50 ng/ml, R&D Systems). Primary neurons were plated at low density (8'000-10'000 cells/well) and kept in an incubator with 5% CO_2 at 37°C. Cultures were grown for 40-48 h before fixation and immunostaining.

Live imaging of cultured intact spinal cords

Live imaging of intact spinal cords was performed as previously described (Dumoulin et al., 2021). Plasmids and dsRNA were injected *in ovo* into the central canal of the neural tube and electroporated unilaterally at either HH13-14 (Cables1 knockdown experiments; 700 ng/µl

Math1::tdTomato-F and 30 ng/µl β-actin::EGFP-F ± 500 ng/µl dsCables1; Figure 3) or HH17 (mRuby3-mCables 1 overexpression; 700 ng/µl Math1::EGFP-F and 1000 ng/µl mRuby3-mCables1; Movie 1) with a BTX ECM830 square-wave electroporator (five pulses at 18 or 25 V with 50 ms duration each) One day later, intact spinal cords were dissected from HH22 embryos and embedded with the ventral side down in a 100-µl drop of 0.5% low-melting agarose-culture medium mix in a 35-mm Ibidi µ-Dish with glass bottom (Ibidi, #81158). Two hundred µl of culture medium (MEM with Glutamax (Gibco)) supplemented with 4 mg/ml Albumax (Gibco), 1 mM pyruvate (Sigma), 100 Units/ml Penicillin and 100 µg/ml Streptomycin (Gibco) were added on top of the agarose drop. Intact spinal cords were incubated for 30 min at 37 °C, 5% CO_2, and 95% air in a PeCon cell vivo chamber before time-lapse recordings were started. Live imaging recordings were acquired with an Olympus IX83 inverted microscope equipped with a spinning disk unit (CSU-X1 10'000 rpm, Yokogawa). Levels of CO_2 and temperature were controlled by the cell vivo temperature controller and the CO_2 controller units (PeCon). For the dsCables1 experiments (Figure 3), 30-40 planes (1.5 µm spacing) of 2x2 binned z-stack images were taken every 15 min for 24 hours with a 20x air objective (UPLSAPO 20x/0.75, Olympus) and an Orca-Flash 4.0 camera (Hamamatsu) with the help of Olympus CellSens Dimension 2.2 software. For the mRuby3-mCables experiment (Movie 1) recordings were performed with a 40x silicone oil objective (UPLSAPO Sx40/1.25, Olympus) with one stack taken every 10 min. Data acquired with 40x magnification were 3D deconvolved with a constrained iterative deconvolution of the Olympus CellSens Dimension 2.2 software (five iterations with adaptive PSF and background removal, Olympus). Z-stacks and maximum projections of z-stack movies were modified and assembled using Fiji/ImageJ (Schindelin et al., 2012). Virtual tracing of single dI1 axons crossing the floor plate (Figure 3) was performed in Fiji using the MtrackJ plugin (Meijering et al., 2012) as previously described (Baeriswyl et al., 2021). Axon behavior was counted as aberrant when instead of turning rostrally there was either caudal turning, stalling, or overshooting at the floor-plate exit site.

ACKNOWLEDGEMENTS

We thank Tiziana Flego and Dr. Beat Kunz for excellent technical assistance. This project was supported by the Swiss National Science Foundation. ES received funding from the University Research Priority Program (URPP) 'Adaptive Circuits in Development and Learning (AdaBD)'.

CONFLICT OF INTEREST

The authors declare no conflict of interest.

REFERENCES

Alther, T.A., Domanitskaya, E., and Stoeckli, E.T. (2016). Calsyntenin 1-mediated trafficking of axon guidance receptors regulates the switch in axonal responsiveness at a choice point. *Development* **143**, 994-1004.

Avilés, E.C., and Stoeckli, E.T. (2016). Canonical wnt signaling is required for commissural axon guidance. *Dev Neurobiol* **76**, 190-208. ¨

Baeriswyl, T. Dumoulin, A., Schaettin, M., Tsapara, G., Niederkofler, V., Helbling, D., Avilés, E., Frei, J.A., Wilson, N.H., Gesemann, M., Kunz, B., and Stoeckli, E.T. (2021). Endoglycan plays a role in axon guidance by modulating cell adhesion. eLife **10**:e64767. doi:10.7554/eLife.64767.

Bashaw, G.J., Kidd, T., Murray, D., Pawson, T., and Goodman, C.S. (2000). Repulsive Axon Guidance: Abelson and Enabled play opposing roles downstream of the roundabout receptor. *Cell* **101**, 703-715.

Bourikas, D., Pekarik, V., Baeriswyl, T., Grunditz, A., Sadhu, R., Nardó, M., and Stoeckli, E.T. (2005). Sonic hedgehog guides commissural axons along the longitudinal axis of the spinal cord. *Nat Neurosci* **8**, 297-304.

Chédotal, A. (2019). Roles of axon guidance molecules in neuronal wiring in the developing spinal cord. *Nat Rev Neurosci*. **20**, 380-396.

De Ramon Francàs, G., Zuñiga, N.R., and Stoeckli, E.T. (2017). The spinal cord shows the way - How axons navigate intermediate targets. *Dev Biol* **432**, 43-52.

Domanitskaya, E., Wacker, A., Mauti, O., Baeriswyl, T., Esteve, P., Bovolenta, P., and Stoeckli, E.T. (2010). Sonic hedgehog guides post-crossing commissural axons both directly and indirectly by regulating Wnt activity. *J Neurosci* **30**, 11167-11176.

Ducuing, H., Gardette, T., Pignata, A., Tauszig-Delamasure, S., and Castellani, V. (2019). Commissural axon navigation in the spinal cord: A repertoire of repulsive forces is in command. *Semin Cell Dev Biol* **85**, 3-12.

Dumoulin, A., Zuñiga, N.R., Stoeckli, E.T. (2021). Axon guidance at the spinal cord midline-A live imaging perspective. *J Comp Neurol* **529,** 2517-2538.

Gorla, M., and Bashaw, G.J. (2020). Molecular mechanisms regulating axon responsiveness at the midline. *Dev Biol* **466**, 12-21.

Hamburger, V., and Hamilton, H.L. (1992). A series of normal stages in the development of the chick embryo. 1951. *Dev Dyn* **195**, 231-272.

Himmels, P., Paredes, I., Adler, H., Karakatsani, A., Luck, R., Marti, H.H., Ermakova, O., Rempel, E., Stoeckli, E.T., and Ruiz de Almodóvar, C. (2017). Motor neurons control blood vessel patterning in the developing spinal cord. *Nat Commun* **8**, 14583.

Kinoshita-Kawada, M., Hasegawa, H., Hongu, T., Yanagi, S., Kanaho, Y., Masai, I., Mishima, T., Chen, X., Tsuboi, Y., Rao, Y., Yuasa-Kawada J., and Wu J.Y. (2019). A crucial role for Arf6 in the response of commissural axons to Slit. *Development* **146***.* dev172106. doi: 10.1242/dev.172106.

Lyuksyutova, A.I., Lu, C.-C., Milanesio, N., King, L.A., Guo, N., Wang, Y., Nathans, J., Tessier-Lavigne, M., and Zou, Y. (2003). Anterior-posterior guidance of commissural axons by Wnt-frizzled signaling. *Science* **302**, 1984-1988.

Mauti, O., Sadhu, R., Gemayel, J., Gesemann, M., and Stoeckli, E.T. (2006). Expression patterns of plexins and neuropilins are consistent with cooperative and separate functions during neural development. *BMC Dev Biol* **6**, 32.

Meijering, E., Dzyubachyk, O.,and Smal, I. (2012). Methods for cell and particle tracking. *Methods Enzymol* **504**, 183-200.

Morenilla-Palao, C., López-Cascales, M.T., López-Atalaya, J.P., Baeza, D., Calvo-Díaz, L., Barco, A., and Herrera, E. (2020). A Zic2-regulated switch in a noncanonical Wnt/βcatenin pathway is essential for the formation of bilateral circuits. *Sci Adv* **6***,* eaaz8797. doi: 10.1126/sciadv.aaz8797.

Niederkofler, V., Baeriswyl, T., Ott, R., and Stoeckli, E.T. (2010). Nectin-like molecules/SynCAMs are required for post-crossing commissural axon guidance. *Development* **137**, 427-435.

Onishi, K., and Zou, Y. (2017). Sonic Hedgehog switches on Wnt/planar cell polarity signaling in commissural axon growth cones by reducing levels of Shisa2. *eLife* **6***,* e25269. doi:10.7554/eLife.25269.

Perrin, F.E., Rathjen, F.G., and Stoeckli, E.T. (2001). Distinct subpopulations of sensory afferents require F11 or axonin-1 for growth to their target layers within the spinal cord of the chick. *Neuron* **30**, 707-723.

Perrin, F.E., and Stoeckli, E.T. (2000). Use of lipophilic dyes in studies of axonal pathfinding in vivo. *Microsc Res Tech* **48**, 25-31.

Philipp, M., Niederkofler, V., Debrunner, M., Alther, T., Kunz, B., and Stoeckli, E.T. (2012). RabGDI controls axonal midline crossing by regulating Robo1 surface expression. *Neural Dev* **7**, 36.

Pignata, A., Ducuing, H., Boubakar, L., Gardette, T., Kindbeiter, K., Bozon, M., Tauszig-Delamasure, S., Falk, J., Thoumine, O., and Castellani, V. (2019). A Spatiotemporal Sequence of Sensitization to Slits and Semaphorins Orchestrates Commissural Axon Navigation. *Cell Rep* 29, 347-362.e5.

Rhee, J., Buchan, T., Zukerberg, L., Lilien, J., and Balsamo, J. (2007). Cables links Robo-bound Abl kinase to N-cadherin-bound beta-catenin to mediate Slit-induced modulation of adhesion and transcription. *Nat Cell Biol* **9**, 883-892.

Schindelin, J., Arganda-Carreras, I., Frise, E., Kaynig, V., Longair, M., Pietzsch, T., Preibisch, S., Rueden, C., Saalfeld, S., Schmid, B., Tinevez, J.Y., White, D.J., Hartenstein, V., Eliceiri, K., Tomancak, P., and Cardona, A. (2012). Fiji: an open-source platform for biological-image analysis. *Nat Methods* **9**, 676-682.

Stoeckli, E.T. (2018). Understanding axon guidance. Are we nearly there yet? *Development* **145***:*dev151415. doi: 10.1242/dev.151415.

Stoeckli, E.T., and Landmesser, L.T. (1995). Axonin-1, Nr-CAM, and Ng-CAM play different roles in the in vivo guidance of chick commissural neurons. *Neuron* **14**, 1165-1179.

Stoeckli, E.T., Sonderegger, P., Pollerberg, G.E., and Landmesser, L.T. (1997). Interference with axonin-1 and NrCAM interactions unmasks a floor-plate activity inhibitory for commissural axons. *Neuron* **18**, 209-221.

van Amerongen, R. (2012). Alternative Wnt pathways and receptors. *Cold Spring Harb Perspect Biol* **4**:a007914. doi:10.1101/cshperspect.a007914.

Wilson, N.H., and Stoeckli, E.T. (2011). Cell type specific, traceable gene silencing for functional gene analysis during vertebrate neural development. *Nucleic Acids Res* **39**, e133.

Wilson, N.H., and Stoeckli, E.T. (2012). In ovo electroporation of miRNA-based plasmids in the developing neural tube and assessment of phenotypes by DiI injection in open-book preparations. *Journal of visualized experiments : JoVE* **68**:4384. doi: 10.3791/4384.

Wilson, N.H., and Stoeckli, E.T. (2013). Sonic hedgehog regulates its own receptor on postcrossing commissural axons in a glypican1-dependent manner. *Neuron* **79**, 478-491.

Yang, T., Huang, H., Shao, Q., Yee, S., Majumder, T., and Liu, G. (2018). miR-92 Suppresses Robo1 Translation to Modulate Slit Sensitivity in Commissural Axon Guidance. *Cell Rep* **24**, 2694-2708.e6.

Zhang, H., Duan, H.O., Kirley, S.D., Zukerberg, L.R., and Wu, C.-L. (2005). Aberrant splicing of cables gene, a CDK regulator, in human cancers. *Cancer Biol Ther* **4**, 1211-1215.

Zukerberg, L.R., Patrick, G.N., Nikolic, M., Humbert, S., Wu, C.L., Lanier, L.M., Gertler, F.B., Vidal, M., van Etten, R.A., and Tsai, L.H. (2000). Cables links Cdk5 and c-Abl and facilitates Cdk5 tyrosine phosphorylation, kinase upregulation, and neurite outgrowth. *Neuron* **26**, 633-646.

Figures and Table

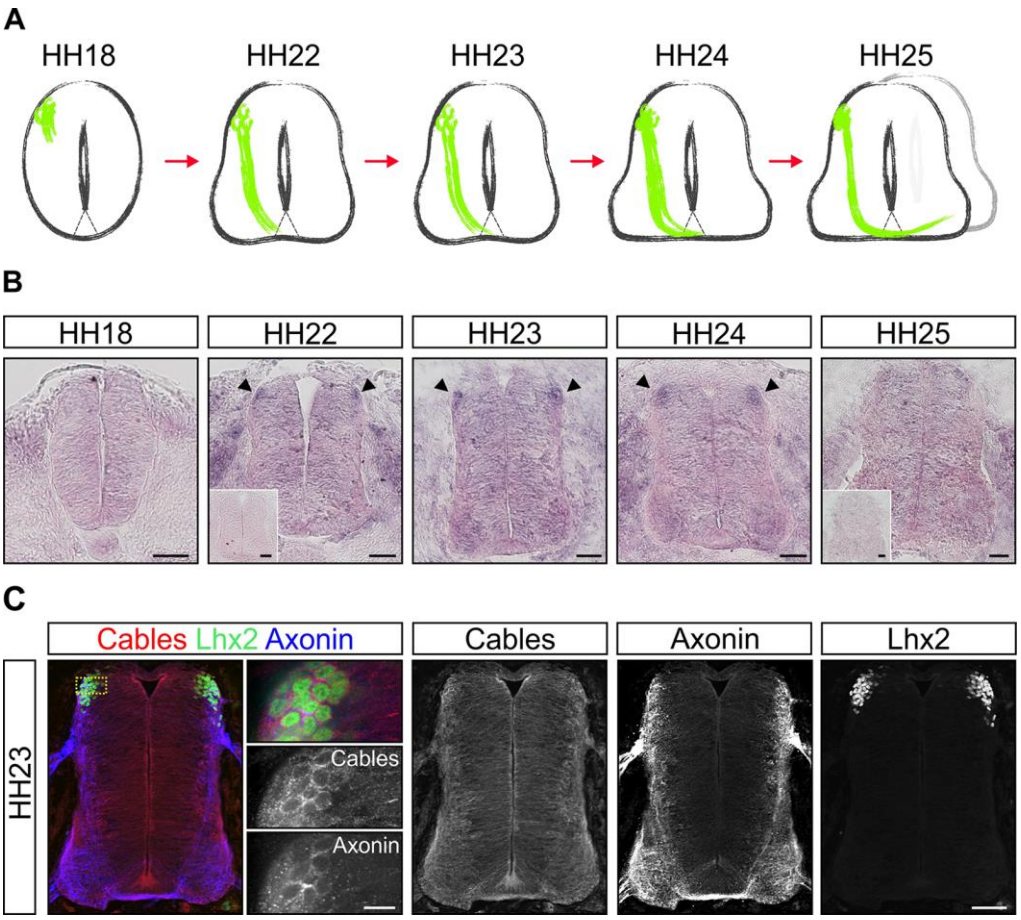

Fig. 1. Cables1 is upregulated in dI1 commissural neurons during axonal midline crossing

Expression of Cables1 mRNA is shown in relationship to the temporal development of the dI1 subpopulation of commissural neurons (A). At HH18, dI1 commissural neurons start to extend their axons in the dorsal spinal cord. They reach and enter the floor plate at HH22. At HH24, axons exit the floor plate and turn rostral along the contralateral side of the floor plate. (B) Cables1 mRNA is expressed at low levels throughout the developing neural tube. Higher levels are found in dI1 commissural neurons between HH22 and HH24 (arrowheads), the time window of midline crossing and axonal turning into the longitudinal axis. Expression levels in dI1 neurons decrease after midline navigation at HH25. Insert shows hybridization with the sense probe. Immunostaining with an anti-Cables antibody confirms its ubiquitous expression in the developing spinal cord at HH23, when dI1 commissural axons cross the ventral midline (C). Cables is also found in axons crossing the floor plate, labeled with an anti-Axonin1 (Contactin2) antibody. Co-staining with an anti-Lhx2 antibody demonstrates expression of Cables1 protein in dI1 neurons. Scale bar: 50 µm in B and C; 10 µm in the higher magnification images in C.

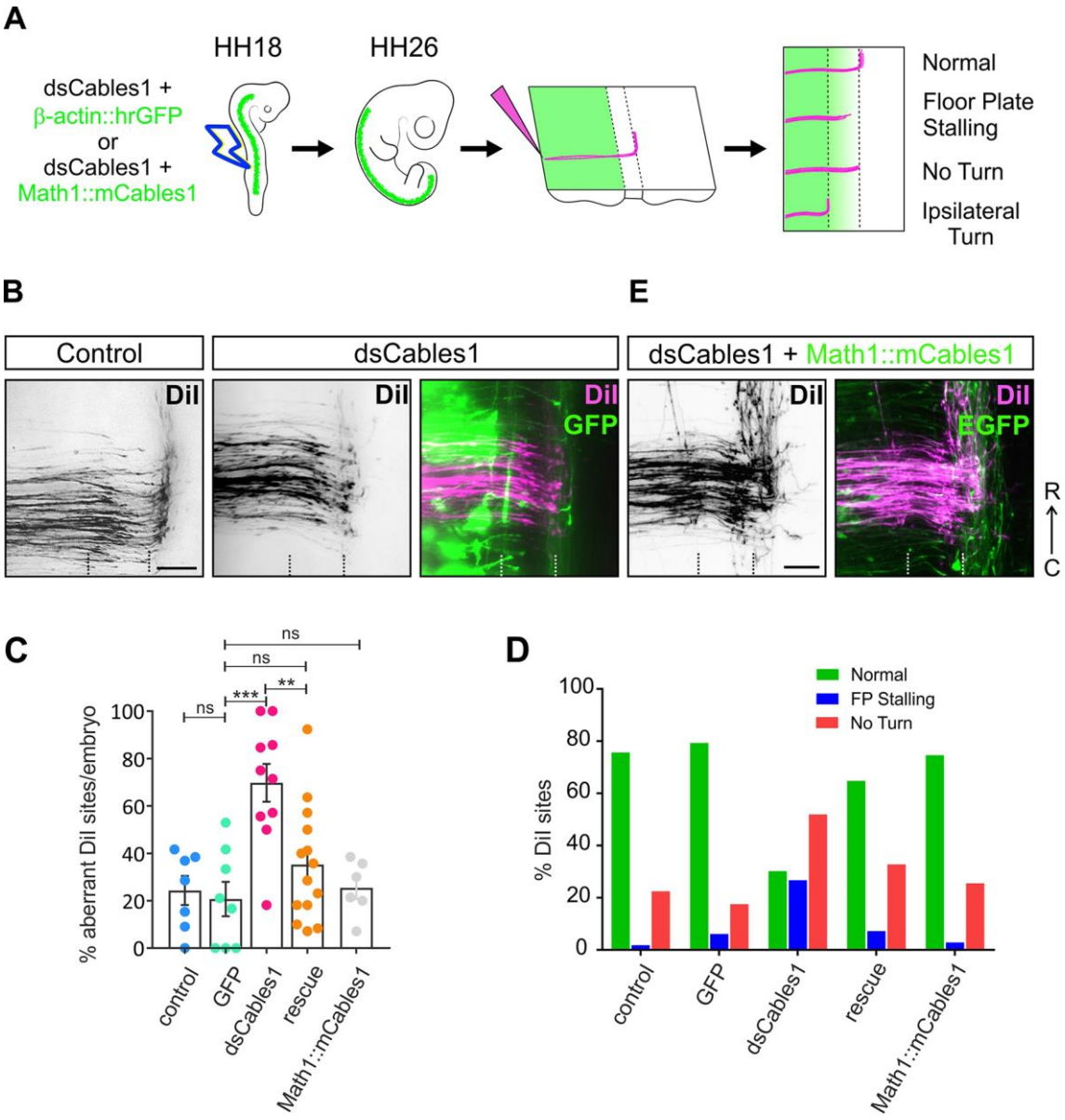

Fig. 2. Cables1 is required for commissural axon navigation at the floor plate

(A) Schematic representation of the loss-of-function experiments using in ovo RNAi at HH18. Embryos were injected with dsRNA derived from Cables1 and a plasmid encoding GFP to visualize the electroporated area of the neural tube. The trajectory of dI1 commissural axons was traced by DiI injected into open-book preparations of embryos dissected at HH26 (see Experimental Procedures for details). For rescue experiments, the embryos were co-injected with dsCables1 and a plasmid encoding mouse Cables1 (mCables1), which was not targeted by the dsRNA derived from chicken Cables1, under the control of the Math1 enhancer for specific expression in dI1 neurons. (B) In control embryos (both untreated controls (not shown) and GFP-expressing control embryos), dI1 commissural axons cross the floor plate (indicated by dashed lines) and turn rostral along the

contralateral floor-plate border. After silencing Cables1, most axons failed to cross the floor plate and did not turn into the longitudinal axis. (C) Quantification of the DiI injection sites with aberrant axon navigation as detailed in the Experimental Procedures. The percentage of DiI injection sites with aberrant axon pathfinding did not differ when GFP-expressing control embryos (20.7±7.2%; N=8 embryos; n=93 DiI injection sites) were compared to untreated controls (24.3±6.1%; N=7; n=92). In contrast, silencing Cables1 induced aberrant axon navigation at 69.8±8.0% of the DiI injection sites (N=10; n=103; ***p=0.0002). (D) Axons in embryos electroporated with dsCables1 mainly failed to turn along the contralateral floor-plate border, although also stalling in the floor plate was much more common than in control embryos. (E) The effect of Cables1 downregulation on axonal navigation was specific, because the co-injection and electroporation of dsCables1 together with the plasmid encoding mouse Cables1 prevented the axon guidance defects seen in the absence of Cables1. When mouse Cables1 was replacing chicken Cables1, only 35.2±6.5% of the DiI injection sites showed aberrant axonal navigation (N=14; n= 160). This value was not significantly different (ns) from the control groups, but significantly different from the dsCables1 group (**p=0.0035). Values are given as mean±s.e.m. One-way ANOVA with Tukey's multiple comparisons test. The numbers of embryos (N) and injection sites (n) are given in parenthesis.

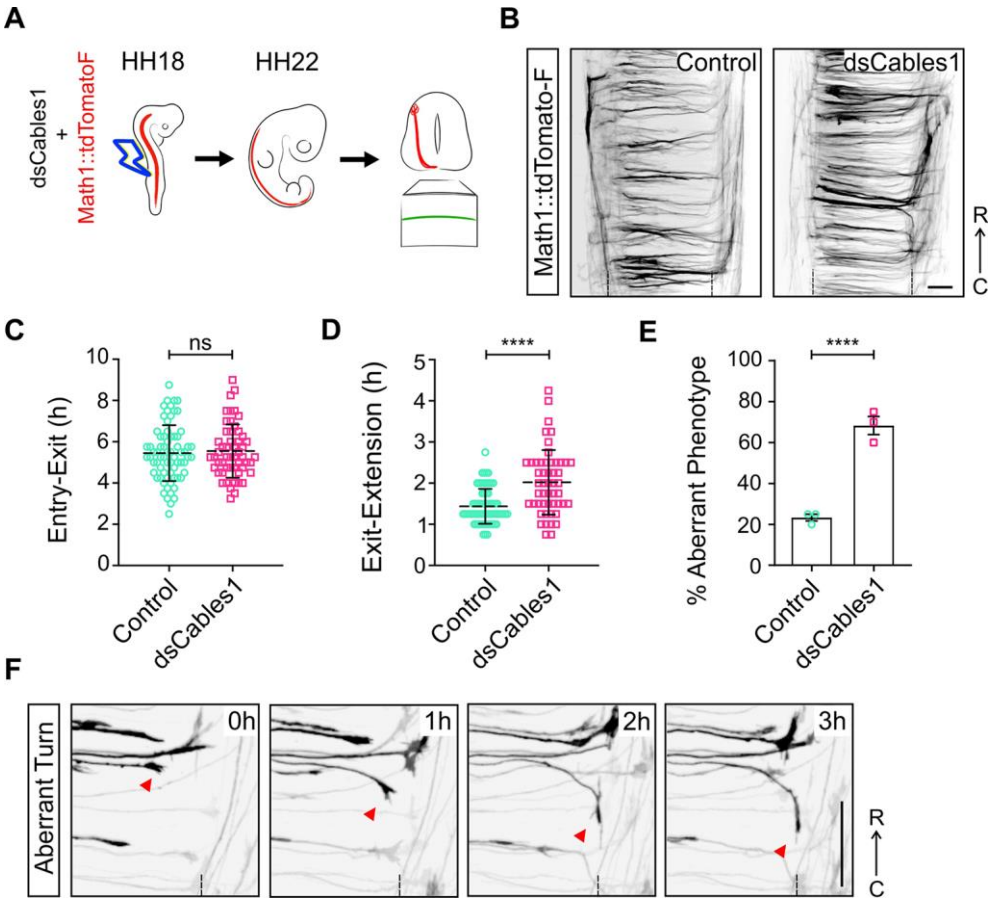

Fig. 3. Live imaging of dI1 commissural axons confirms turning errors of post-crossing commissural axons after silencing Cables1

(A) Schematic drawing depicting the design of the live imaging experiment to visualize dI1 axons crossing the ventral midline of the spinal cord in real time. First, spinal cords were unilaterally electroporated in ovo at HH13-14 with the dI1-specific reporter plasmid Math1::tdTomatoF with or without dsCables1. One day later, intact spinal cords were dissected at HH22, cultured with the ventral midline down and imaged for 24 hours (1 stack every 15 min) with an inverted spinning disk microscope. (B) Examples of a temporal projection from a 24-hour time lapse recording of a control- and a dsCables1-treated spinal cord, showing disorganization of the post-crossing segment after Cables1 silencing compared to control (black arrowheads). (C) Quantification of average time of floor-plate crossing by dI1 axons did not show any difference in absence of Cables1 compared to control. N(embryos) = 3 for each condition; n(axons) = 70 (control) and 53 (dsCables1): unpaired t-test. (D) However, the time dI1 axons took at the floor-plate exit site to start extending along the longitudinal axis was significantly longer in the absence of Cables1 compared to control. N(embryos) = 3 for each condition; n(axons) = 69 (control) and 51 (dsCables1); unpaired t-test. (E) Quantification

of navigation behavior at the single axon level visualized by live imaging revealed an increase of aberrant phenotypes at the floor-plate exit site, when Cables1 was downregulated. N(embryos) = 3 for each condition; n(axons) = 60 for each condition; unpaired t-test. $p<0.0001$ (****), $p<0.001$ (***), and $p\geq0.05$ (ns) for all tests. (F) Example of a dI1 axon turning caudally instead of rostrally at the floor-plate exit site (red arrowhead) after downregulation of Cables1. Dashed lines represent the floor-plate boundaries (B) or exit (F). R, rostral; C, caudal. Scale bars: 50 µm.

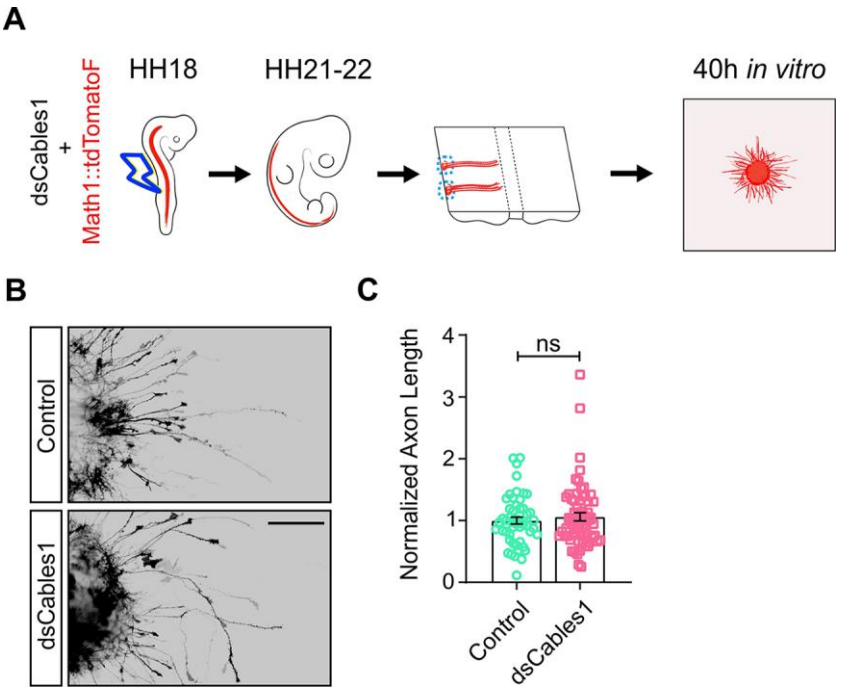

Fig. 4. Cables1 is not required in pre-crossing axons

We excluded an effect of Cables1 on pre-crossing axons *in vitro*. HH18 embryos were injected and electroporated with Math1::td-Tomato-F (farnesylated td-Tomato under the control of the Math1 enhancer for specific expression in dI1 neurons) alone or together with dsRNA derived from Cables1 (dsCables1). Explants of dorsal commissural neurons (blue circles) were prepared from open-book preparations of spinal cords dissected from HH21/22 embryos and cultured for 40 h (A). Axon outgrowth was visualized by staining for RFP (B). The average lengths of commissural axons were normalized to the lengths of control explants for each experiment (C). A total of 52 control explants (from 13 different embryos) and 64 explants taken from embryos electroporated with dsCables1 (n=16 embryos) from three independent experiments were quantified. The average length of neurites from control explants was 173 µm. See Methods for details. We did not find any significant difference (ns; p=0.4968) in neurite length (unpaired t-test). Scale bar: 200 µm.

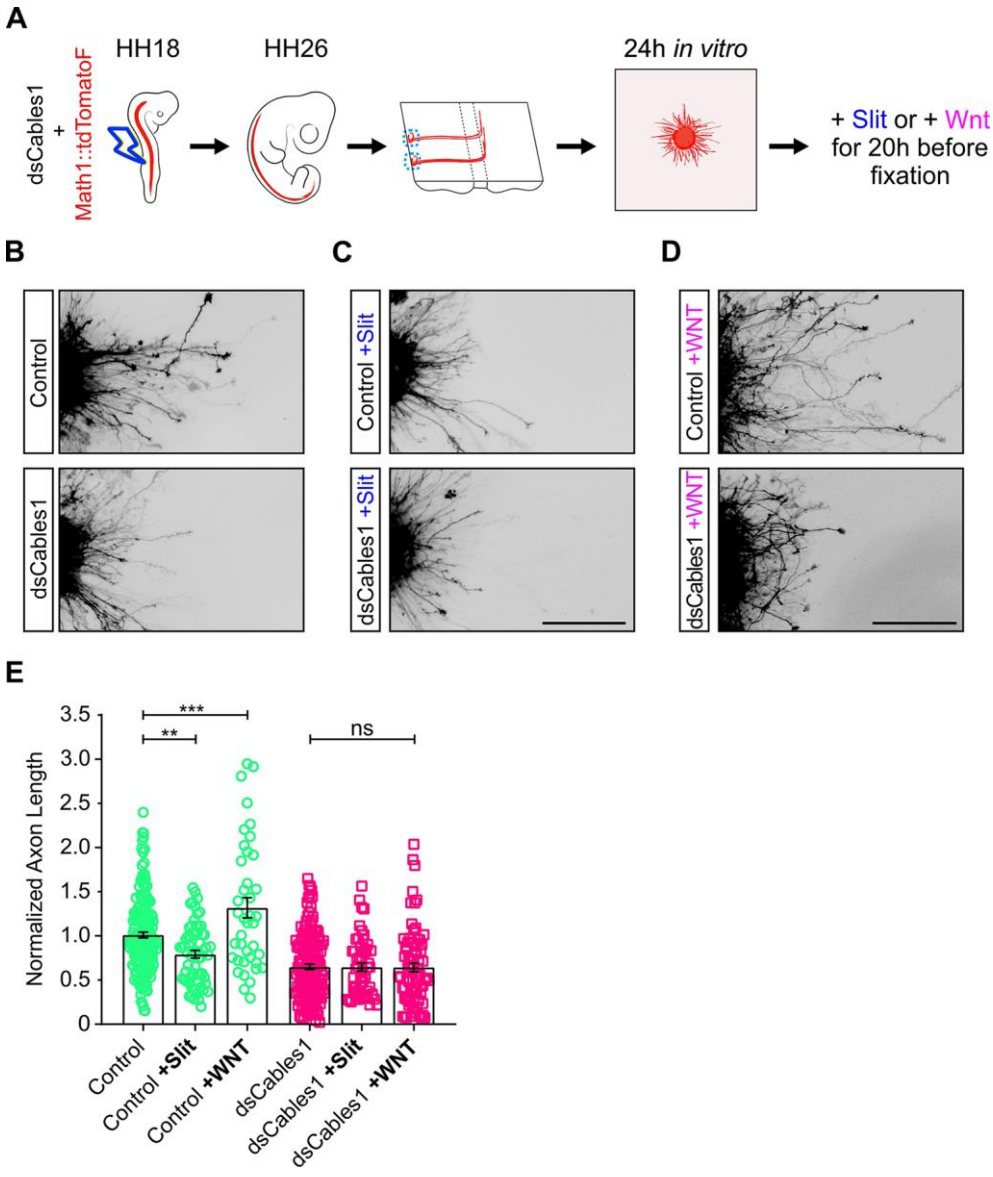

Fig. 5. Loss of Cables1 prevents responsiveness to Slit and Wnt5a

Schematic representation of the experimental set-up (A). HH18 embryos were electroporated with Math1::td-Tomato alone or in combination with dsRNA derived from Cables1 (dsCables1). Explants of dI1 commissural neurons (blue circles) were prepared from open-book preparations of spinal cords dissected from HH26 embryos and cultured for 24 h before either medium alone (control; B), Slit2 (200 ng/ml; C), or Wnt5a (200 ng/ml;D) were added to the cultures for another 20 h. Explants were fixed and stained to visualize RFP. For each experiment, neurite lengths were measured and normalized to the length of control explants (E). Data from three independent experiments are pooled. For control explants, the presence of Slit2 reduced the average axon length by 21% (n=16; C upper panel compared to B, upper panel). In contrast, the presence of Wnt5a increased average

axon length by 32% (n=10; D upper panel). In contrast, axons from explants with neurons electroporated with dsCables1 did not respond to either Slit2 (n=13; C lower panel) or Wnt5a (n=20; D lower panel). ns, not significant; **p=0.0065; ***p=0.0007; One-way ANOVA with Tukey's multiple comparisons test. Scale bar: 200 µm.

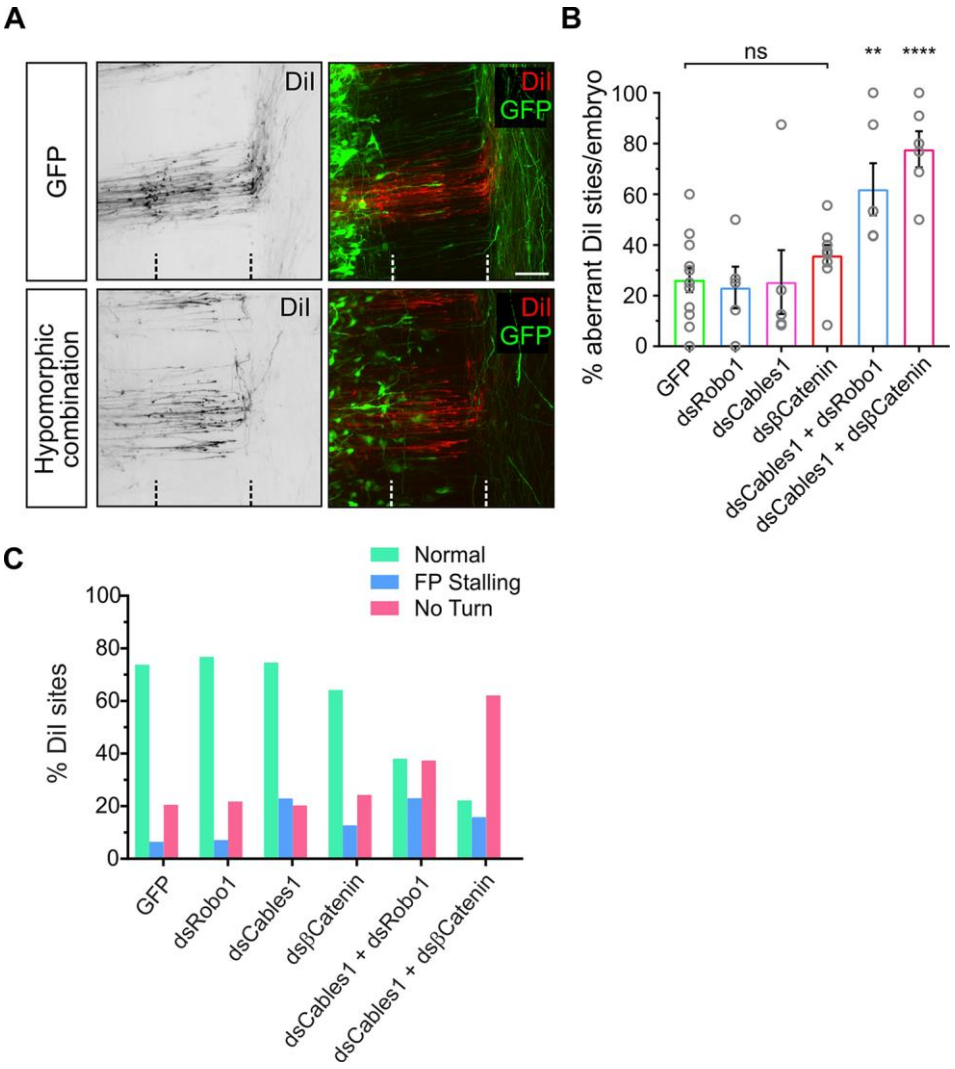

Fig. 6. Cables1 cooperates with Slit/Robo and Wnt/Fzd signaling in axon guidance at the midline

Open-book preparations of control-treated (GFP-expressing) embryos and embryos electroporated with low concentrations of dsRNA derived from Cables1, Robo1, or β-Catenin alone or in combination were analyzed for axon guidance at the floor plate. In control-treated embryos, axons were crossing the midline and turning rostral upon floor-plate exit (A). In contrast, axons failed to turn correctly or did not reach the floor-plate exit site in embryos treated with combinations of any two low concentrations of dsCables1, dsRobo1, or dsβ-Catenin. (B) Compared to GFP-expressing control embryos, where an average of 26.2±4.8% of DiI injection sites with aberrant axonal trajectories were found (n=125, N=12), injection of only 75 ng/µl of dsRNA did not induce any aberrant axon guidance: dsRobo (23.2±8.2%; n=63 injection sites from N=5 embryos), dsCables1 (25.4±12.5%; n=56, N=6), dsβCatenin (35.8±4.1%; n=85, N=9). However, aberrant axonal navigation was found when combinations of dsRNA were used: dsCables1 + dsRobo1 (62.0±10.2%; n=85, N=6); dsCables1 + dsβCatenin (77.8±7.7%; n=70, N=6). ns not significant, **p<0.01, ****p=0.0001. One-way ANOVA with Dunnett's multiple comparisons test. Scale bar: 50 µm.

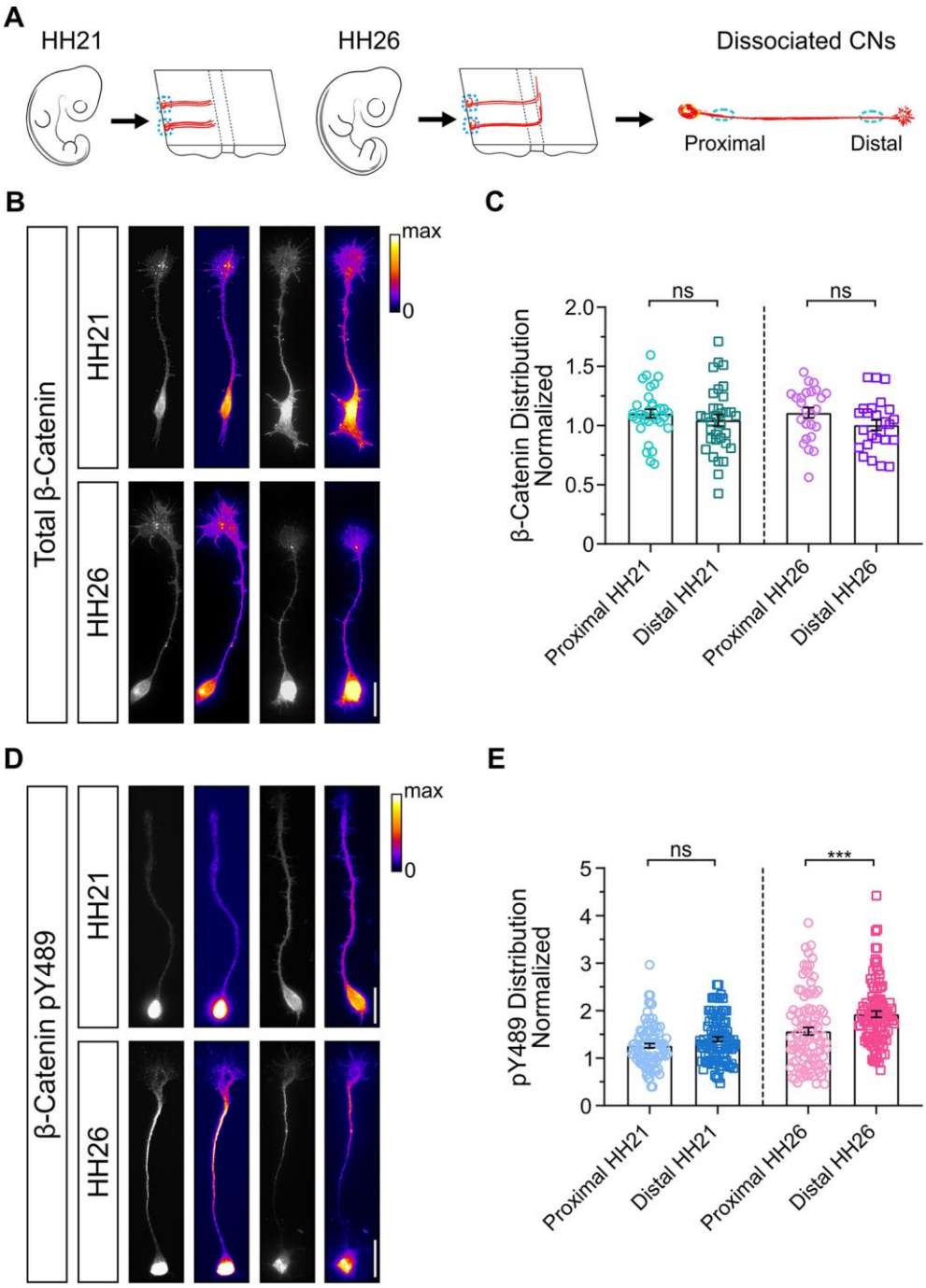

Fig. 7. β-Catenin pY489 accumulates in the distal part of post-crossing commissural axons.

(A) Schematic representation of the experimental design. Dissociated commissural neurons were prepared from open-book preparations of HH21 and HH26 embryos, grown for 40-48 h before staining with antibodies recognizing β-Catenin or specifically β-Catenin pY489. Fluorescence intensity in the proximal and distal parts of the axons were measured and normalized to the average intensity of the entire axon. Total levels of β-Catenin measured at HH21 and HH26 did not differ between the proximal and the distal axon (B,C; HH21, n=33 neurons; HH26, n=25 neurons). Similarly, comparing

levels of β-Catenin pY489 between proximal and distal axons of axons collected from HH21 embryos did not differ (D,E). In contrast, levels of β-Catenin pY489 were significantly higher in distal compared to proximal axons of neurons collected from HH26 embryos (D,E; HH21, n=95 neurons; HH26, n= 99 neurons; p=0.0538 for HH21 and ***p=0.0009 for HH26). Results were obtained from three independent experiments. For each condition, two examples are shown in (B) and (C) demonstrating that the distribution between proximal and distal axons was consistent even when staining intensities varied between experiments. ns=not significant; Paired t-test.

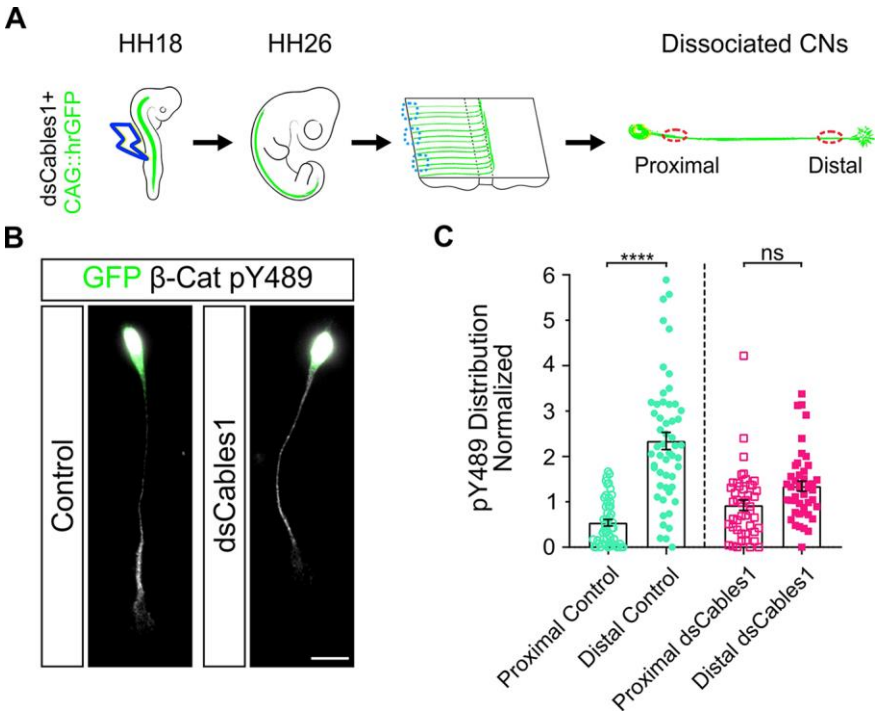

Fig. 8. Cables1 regulates the phosphorylation of β-Catenin Y489 in post-crossing commissural axons.

(A) Schematic of the experimental design. HH18 embryos were electroporated with dsRNA derived from Cables1 and a GFP reporter plasmid. Dissociated commissural neurons were prepared from open-book preparations of HH26 spinal cords, stained with an antibody specific for β-Catenin pY489 and used for intensity measurements. (B) Immunostaining of commissural neurons for β-Catenin pY489 isolated from control-treated and dsCables1-electroporated embryos demonstrated that the accumulation of β-Catenin pY489 depended on Cables1, as intensity levels did no longer significantly differ when we compared distal and proximal axons from embryos lacking Cables1. (C) Quantification of β-Catenin pY489 levels in proximal compared to distal axons in control and dsCables1-deficient neurons normalized to the average intensity of the entire axons (±s.e.m.). Results were obtained from three independent experiments. Control, n=53 neurons; dsCables1, n=45 neurons. Control, ****p<0.0001; dsCables1, ns, p=0.1382; separate t-test for control and dsCables group. The results presented here are not directly comparable to those shown in Figure 7E, because the cultures were not stained with the same batch of anti- β-Catenin pY489 antibodies. Therefore, the difference in proximal compared to distal control levels are not the same as those shown in Figure 7E.

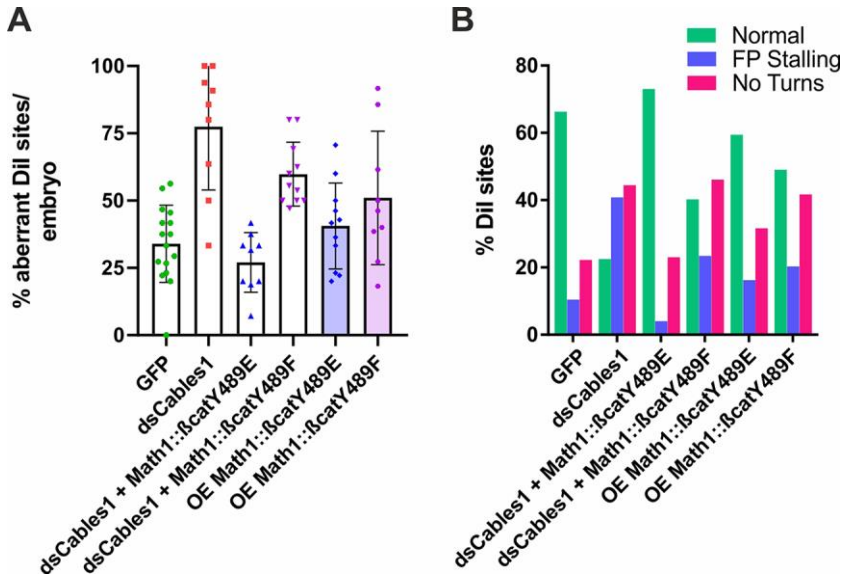

Fig. 9. β-CateninY489E, a constantly active mutant of β-CateninY489, rescues aberrant turning behavior of post-crossing commissural axons

The failure to turn rostral along the contralateral floor-plate border after downregulation of Cables1, seen at 77.5±7.8% of the injection sites (N=9 embryos; n=101 injection sites) compared to GFP-expressing control embryos with aberrant phenotypes at 34.0±3.6% (N=16 embryos, n=192) of the injection sites, was reduced to control levels, when dsCables1 was electroporated together with a plasmid expressing β-CateninY489E, a constantly active mutant of β-CateninY489 (27.0±3.7%; N=9; n=126; A). In contrast, phenotypes induced by downregulation of Cables1 could not be rescued with concomitant expression of β-CateninY489F, a mutant version of β-CateninY489 that cannot be phosphorylated at tyrosine Y489 (59.8±3.6%, N=11, n=123). The injection of the rescue constructs, Math1::β-CateninY489E (40.6±4.8%, N=11, n=135) and Math1::β-CateninY489F (51.0±8.3%, N=9, n=111) in the presence of endogenous β-CateninY489 slightly increased the DiI injection sites with aberrant axon guidance compared to control-treated, GFP-expressing embryos but the changes were not significant (p=0.92 and p=0.18). The values were, however, significantly different from those seen after downregulation of Cables1 (p=0.0002 and p=0.0211, respectively). Qualitative analysis of the phenotypes indicated that expression of β-CateninY489 was not able to rescue the no-turning phenotype seen in the absence of Cables1 (B). The percentage of DiI injection sites with post-crossing axons failing to turn after β-CateninY489 expression in control embryos was higher than controls most likely due to competition with endogenous β-Catenin, despite the fact that the number of normal injection sites was not significantly different from GFP control embryos.

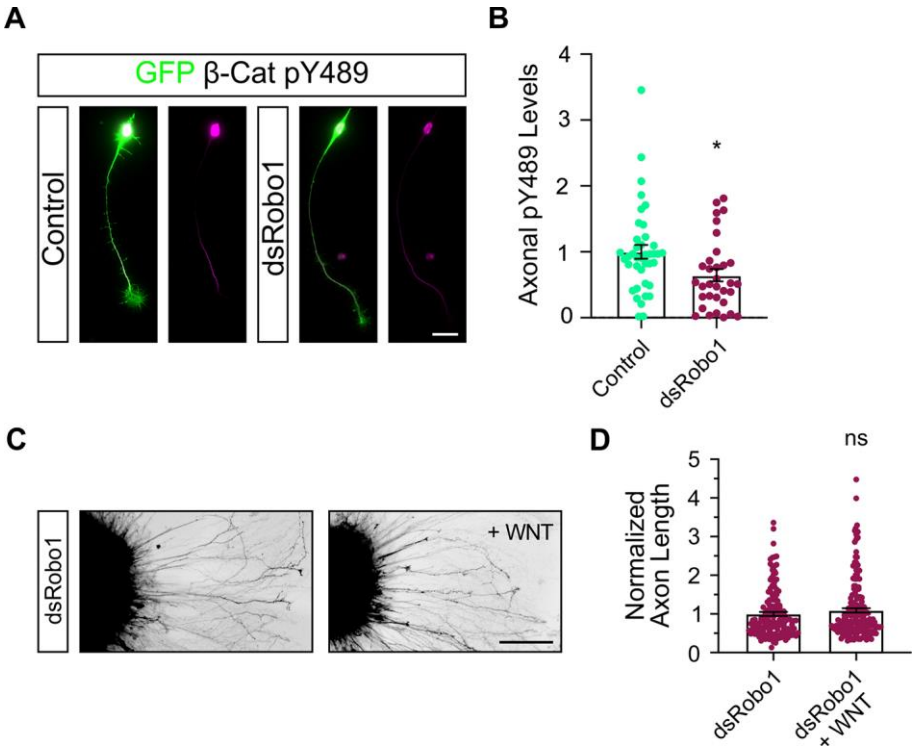

Fig. 10. Robo1 is required for the phosphorylation of β-Catenin at Y489 and the responsiveness of axons to Wnt

To confirm a role of Robo1 in Wnt responsiveness, we stained axons dissected either from HH26 control-treated embryos (electroporation of GFP plasmid alone) or from embryos electroporated with dsRobo1 (A). Levels of phosphorylated β-Catenin (β-Catenin pY489) were reduced in the absence of Robo1 (B). Control, n=40 neurons; dsRobo1, n=33 neurons; *p=0.0145; unpaired t-test. Results were combined from 3 independent experiments. This observation was in line with the failure of axons to respond to Wnt5a (200 ng/ml) added to explants taken from embryos electroporated with dsRobo1 (C). The average axon length in the absence of Robo1 did not increase after addition of Wnt5a (D). dsRobo1, n=45 explants; dsRobo1+Wnt5a, n=51 explants. ns, not significant. Compare Figure 5 for the effect of Wnt5a addition to control explants. Scale bar: 20 µm in A, 200 µm in C.

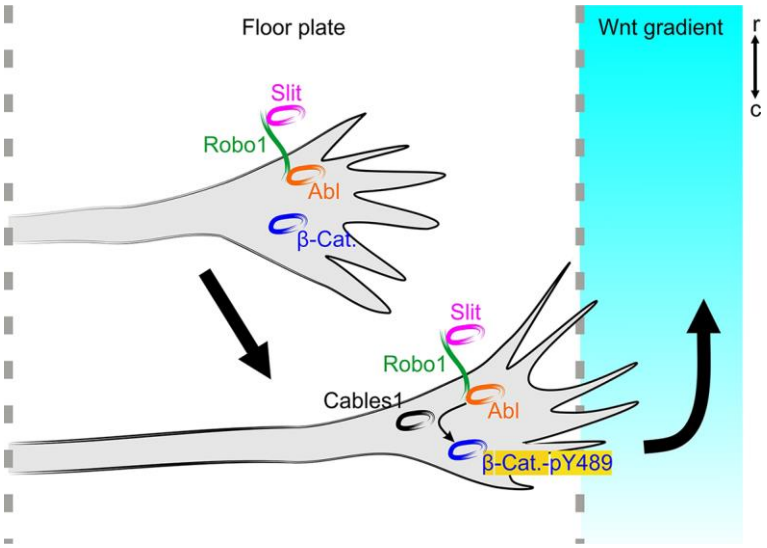

Fig. 11. Cables1 links Robo-mediated floor-plate exit with responsiveness to Wnt signaling by regulating Abl-mediated phosphorylation of β-Catenin

Commissural axons are expelled from the floor plate (indicated by dashed lines) by the midline-associated repellent Slit binding to Robo1 on the growth cone surface. Cables1 controls the exit of commissural axons from the floor plate by transferring Abl kinase from Robo1 to β-Catenin. This results in phosphorylation of β-Catenin at tyrosine 489 (β-Cat pY489) and its accumulation in the distal axon and the central domain of the growth cone. Accumulation of β-Catenin pY489 in the distal axon and growth cone is required for the responsiveness of post-crossing commissural axons to the Wnt gradient.

Table 1

REAGENT or RESOURCE	SOURCE	IDENTIFIER
Antibodies		
Rabbit anti-Cables1, 1:1000 IF	ABCAM	Cat#ab130967 (Discontinued)
Rabbit anti-Cables1, 1:750 WB	Origene	AP06793PU-N
Rabbit anti-GAPDH, 1:2500 WB	ABCAM	Cat#ab9485
Mouse IgM anti-β-Catenin pY489, Supernatant 1:100 IF	Hybridoma Bank	
Rabbit anti-β-Catenin, 1:500 IF	Santa Cruz	Cat#Sc-7199 (Discontinued)
Mouse anti-Lhx2, 1:50 IF	Developmental Studies Hybridoma Bank	PCRP-LHX2-1C11
Mouse anti-Hnf3β, 1:2 IF	Developmental Studies Hybridoma Bank	4C7
Mouse anti-Neurofilament, 1:150 IF	Invitrogen	#RMO-270
Mouse anti-Islet1, 1:10 IF	Developmental Studies Hybridoma Bank	40.2D6
Rabbit anti-Pax2, 1:200 IF	Invitrogen	#71-6000
Rabbit anti-RFP, 1:2000 IF	Antibodies Online	Cat#ABIN129578
Goat anti-Robo3, 1:500 IF	R&D Systems	Cat#AF3076
Rabbit anti-Axonin1/Contactin2, 1:500	Stoeckli and Landmesser, 1995	
Goat anti-GFP-FITC, 1:500 IF	Rockland	Cat#600-102-215
Donkey anti-mouse Cy3, 1:2000 IF	Jackson Immuno Research	Cat#715-165-150
Goat anti-mouse Cy3, 1:2000 IF	Jackson Immuno Research	Cat#115-165-003
Goat anti-mouse IgM TRITC	Cappel	Cat# 55531
Donkey anti-rabbit Cy3, 1:2000 IF	Jackson Immuno Research	Cat#711-165-152
Donkey anti-rabbit Alexa Fluor 488, 1:1000	Invitrogen	Cat#A21206
Anti-DIG-AP, Fab 1:1000 ISH	Roche Diagnostic	Cat#11093274910
Goat anti-rabbit HRP	Jackson Immuno Research	Cat#111-035-003
Chemicals, peptides, and recombinant proteins		
Fast DiI	Thermo Fisher	Cat#D7756
NBT	Axonlab	Cat#A1117,0001
BCIP	Axonlab	Cat#A1243,0001
mSlit2 CF	R&D Systems	Cat#5444-SL
hWnt5a	R&D Systems	Cat#645-WN-010
RhNetrin1 CF	R&D Systems	Cat#6419-N1
PBS pH 7.4	Life Technologies	Cat#10010056
Mowiol 4-88 Reagent	Merck	Cat#475904
Trypsin EDTA 10X	Invitrogen	Cat#15400054
DIG RNA labeling mix	Roche Diagnostic	Cat#11277073910
T7 RNA polymerase	Promega	Cat#P207B
SP6 RNA polymerase	Promega	Cat#P108B

ECL Western Blotting Detection Reagent	GE Healthcare	RPN2209
Q5 High-Fidelity DNA Polymerase	New England Biolabs	Cat#M0491L
Commercial assays		
Q5 Site-Directed Mutagenesis Kit	New England Biolabs	Cat#E0554S
NEBuilder® HiFi DNA Assembly Master Mix	New England Biolabs	Cat#E2621S
SuperScript™ III First-Strand Synthesis SuperMix	Thermo Fisher	Cat#18080-400
Fast Sybr Green Master Mix	Thermo Fisher	Cat#4385610
Experimental models: organisms/strains		
Gallus gallus: Hubbard JA57 strain	Brüterei Stöckli, Ohmstal	N/A
Oligonucleotides		
qPCR chicken *Cables1_X1*-specific primer sequence, forward: TACCCAAGTCGGGGACATGA	Microsynth AG	N/A
qPCR chicken *Cables1_X1*-specific primer sequence, reverse: CGAGTTCCGAGAGCATTGGT	Microsynth AG	N/A
qPCR chicken *Cables1_X2*-specific primer sequence, forward: GGAAAATGCCCCACTACGCA	Microsynth AG	N/A
qPCR chicken *Cables1_X2*-specific primer sequence, reverse: CCAACTTCATGTCCCTGCCAT	Microsynth AG	N/A
qPCR chicken *Cables1_X3*-specific primer sequence, forward: CCCACATTCCCCATTCGCC	Microsynth AG	N/A
qPCR chicken *Cables1_X3*-specific primer sequence, reverse: GGGAGATCAGCCGACGTCTATG	Microsynth AG	N/A
qPCR chicken *Cables2_X1*-specific primer sequence, forward: AGAGAAGGCGTTTTATCTCCCAG	Microsynth AG	N/A
qPCR chicken *Cables2_X1*-specific primer sequence, reverse: GCGCAGATTAATACGATCCTGCTG	Microsynth AG	N/A
qPCR chicken *18S*-specific primer sequence, forward: CGAAAGCATTTGCCAAGAAT	Himmels et al.,2017	
qPCR chicken *18S*-specific primer sequence, reverse: GGCATCGTTTATGGTCGG	Himmels et al.,2017	
Recombinant DNA		
ChEST446e14 (Cables1)	Source BioScience	
ChEST809a5 (Cables 2)	Source BioScience	
ChEST822o14 (Cables 1)	Source BioScience	
ChEST231k15 (β-Catenin)	Source BioScience	
CAG::HA-hRobo1-myc	Philipp et al., 2012	
CAG::mRuby3-mCables	This paper	
β-actin::EGFP-F	Baeriswyl et al., 2021	
β-actin::miβ-Catenin_IRES-EBFP	Avilés and Stoeckli, 2016	
Math1::tdTomato-F	Wilson and Stoeckli, 2013	
Math1::EGFP-F	Wilson and Stoeckli, 2013	
pCAGGs::hrGFP	Wilson and Stoeckli, 2011	
Math1::mCables1-myc_IRES-EGFP	This paper	
CAG::mβ-Catenin-myc_IRES-EGFP	This paper	
Math1::mβ-CateninY489E-myc_IRES-EGFP	This paper	

Math1::mβ-CateninY489F-myc_IRES_EGFP	This paper	
Software		
ImageJ	Schneider et al., 2012	https://imagej.nih.gov/ij/
Prism 8	GraphPad	https://www.graphpad.com/scientific-software/prism/;%20RRID:%20SCR_002798/

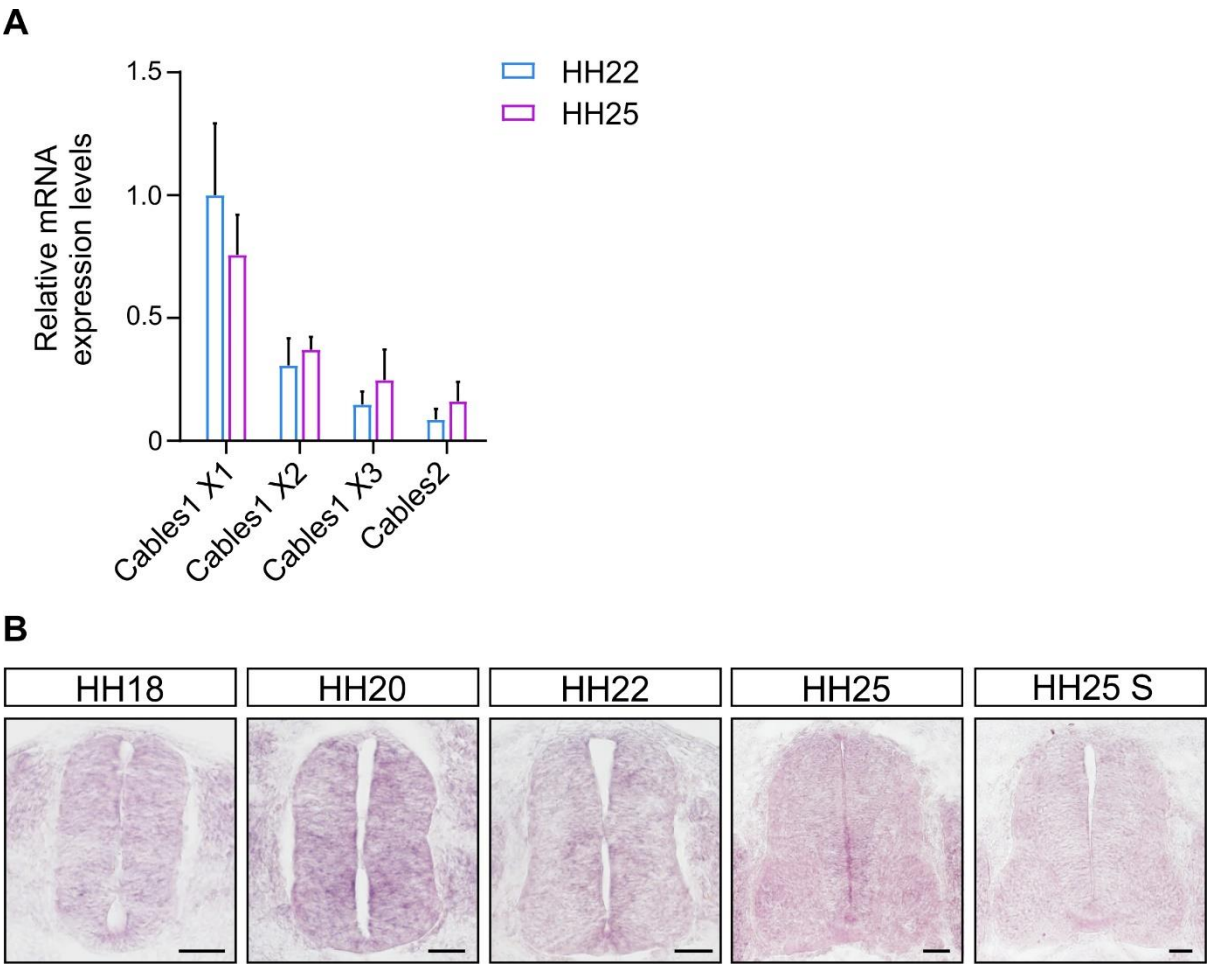

Fig. S1. In the developing spinal cord, Cables2 is expressed at very low levels, if at all

qRT-PCR analysis showed high expression levels of Cables1 isoformX1 in comparison to Cables1 isoformX2 and isoformX3, as well as Cables2 at stages HH22 and HH25. All mRNA levels were normalized to Cables1 isoformX1 at HH22 (A). If at all, Cables2 mRNA was found at very low levels throughout the developing neural tube during the time window, when dI1 commissural axons cross the floor plate and turn rostral along the contralateral floor-plate border (compare sections hybridized with anti-sense probe to the section hybridized with the sense probe (last panel labeled S)). In contrast to what we observed for Cables1 mRNA (Figure 1), Cables2 mRNA was not upregulated in dI1 commissural neurons during the time when their axons cross the midline (B). Scale bar: 50 µm.

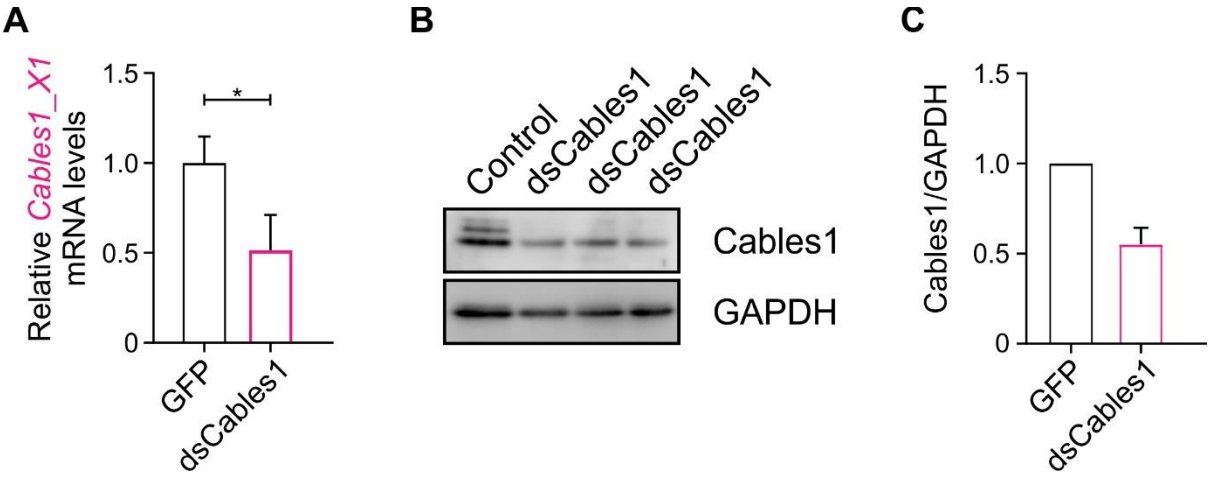

Fig. S2. Downregulation of Cables1 by in ovo RNAi effectively reduces levels of Cables1 mRNA and protein.

Effective downregulation of Cables mRNA was demonstrated with qRT-PCR for isoform X1 (A) with 4 pools of embryos sacrificed at HH23 (A). *p=0.03, paired t-test. Western blotting of proteins isolated from HH25 spinal cords confirmed effective downregulation of Cables1 in three independent pools of embryos electroporated with dsCables1 at HH17/18 (B). Levels were reduced by 50-60%. With the parameters used to silence Cables1, we successfully electroporated on average 53% (range 45-60%) of the cells in the targeted area of the neural tube. Therefore, the observed reduction in Cables1 protein indicate a more or less complete removal of Cables1 from the electroporated cells.

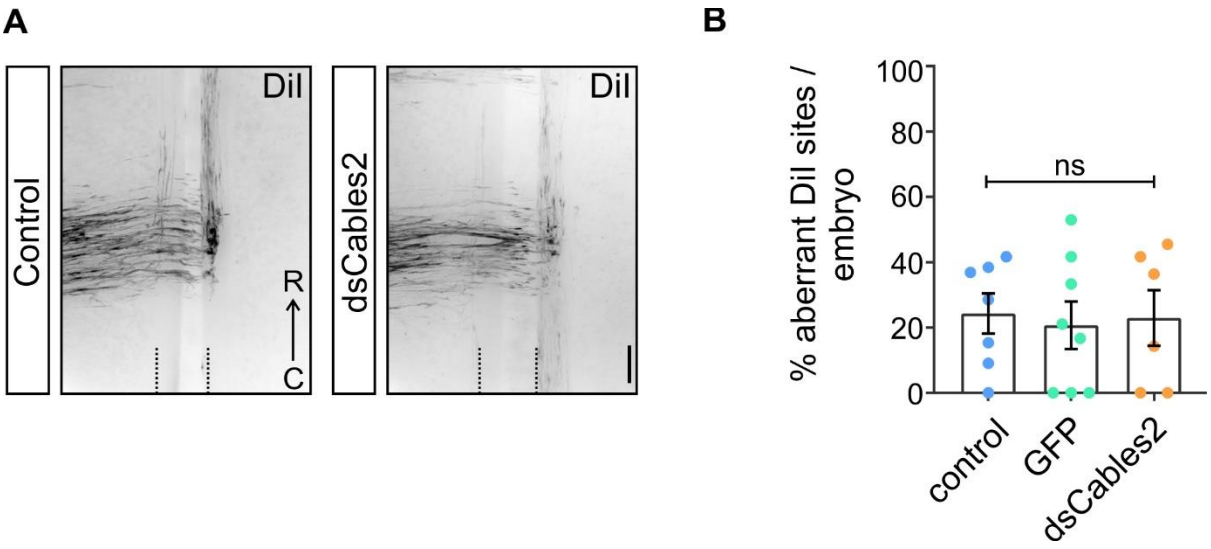

Fig. S3. Downregulation of Cables2 does not impact commissural axon guidance.

Functional analysis of Cables2 revealed no effect on dI1 axon guidance at the floor plate (A). Quantification of aberrant commissural axon trajectories in non-injected control embryos (control, 24.3 ±6.1%; n=92 injection sites in N=7 embryos), GFP-expressing control embryos (GFP; 20.7±7.2%; n=93, N=8), and embryos electroporated with dsRNA derived from Cables2 (dsCables2; 23.0±8.4%; n=55, N=6) showed no significant (ns) difference in the number of DiI injection sites with aberrant axonal trajectories (B). Both untreated and GFP-expressing controls are the same as those shown in Figure 2. Values are given as mean ± s.e.m. One-way ANOVA with Tukey's multiple comparisons test. Scale bar: 50 µm.

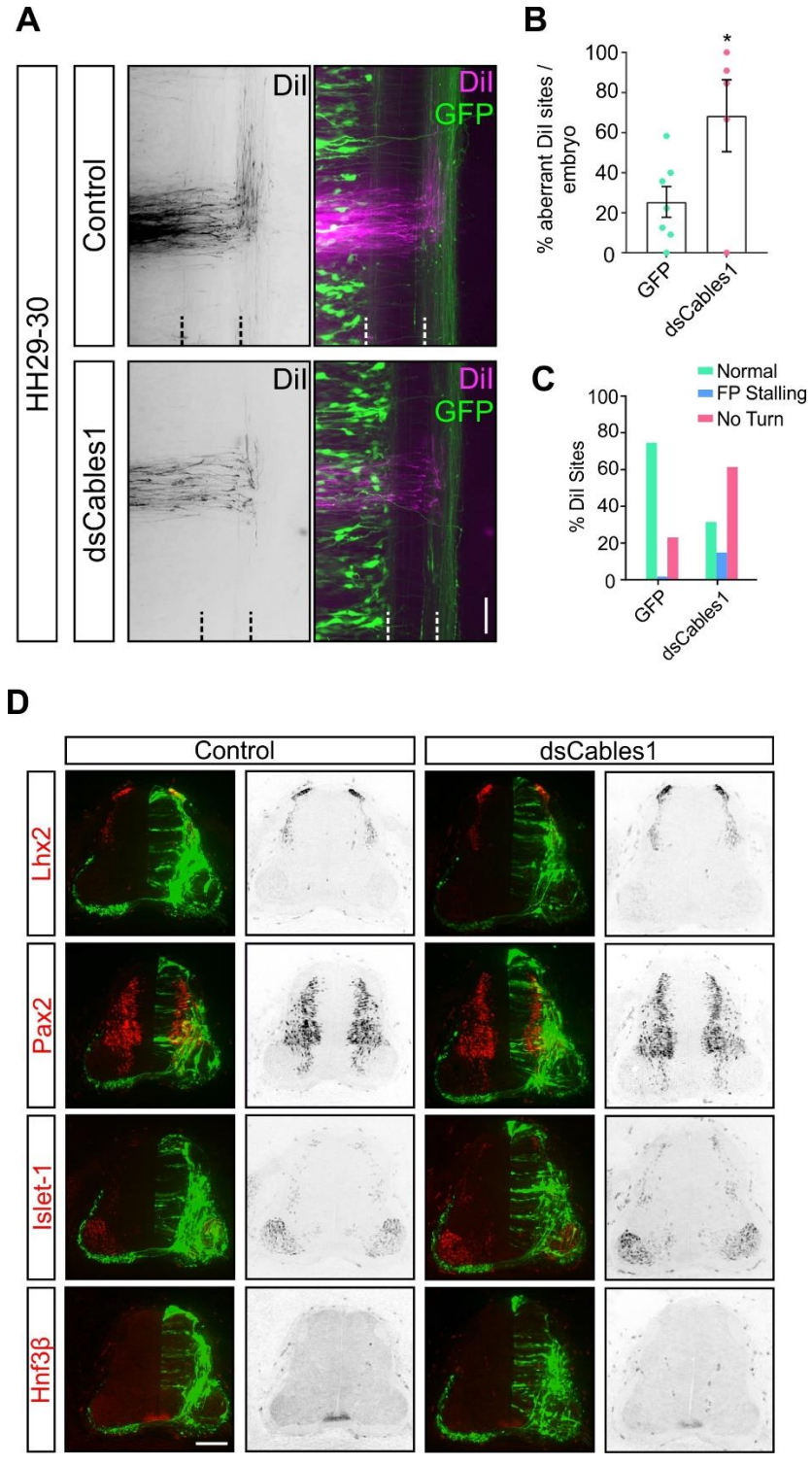

Fig. S4. The axon guidance defects observed after silencing Cables1 are not explained by a reduction in neurite growth speed or due to defects in patterning.

To exclude a slower growth rate as the reason for the failure of axons to turn into the longitudinal axis in the absence of Cables1, we analyzed dI1 axonal navigation at the floor plate in open-book preparations of spinal cords dissected from embryos at HH29/30, that is 1.5 days older than those shown in Figure 2. The fact that axons still stalled at the floor-plate exit site and failed to turn into the longitudinal axis confirmed that axon guidance defects could not be explained by a slower growth rate, but had to be due to a failure to respond to guidance cues provided by the floor plate (A). (B) When compared to control-treated embryos, aberrant axon guidance was found at 68.4±17.9% of the DiI injection sites in embryos electroporated with dsCables1 (n=56 injection sites in N=5 embryos), compared to control-injected embryos (GFP plasmid only), where aberrant axonal trajectories were seen only at 25.4±7.7% of the injection sites (* p=0.0338; n=74 injection sites in 7 control-injected embryos; unpaired t-test). In contrast to GFP-expressing control embryos, embryos electroporated with dsCables showed an increase in the number of DiI injection sites with axons either stalling in the floor plate, or not turning into the longitudinal axis at the floor-plate exit site (C). Scale bar: 50 µm. Immunostaining of HH25 spinal cord sections with antibodies against Lhx2 (marker for dI1 neurons), Pax2 (interneurons), Islet-1 (motoneurons), and Hnf3β (floor-plate cells) did not reveal any differences in neuronal differentiation between control-treated, GFP-expressing controls, and experimental embryos electroporated with dsRNA derived from Cables1 at HH18 (D). Scale Bar: 100 µm.

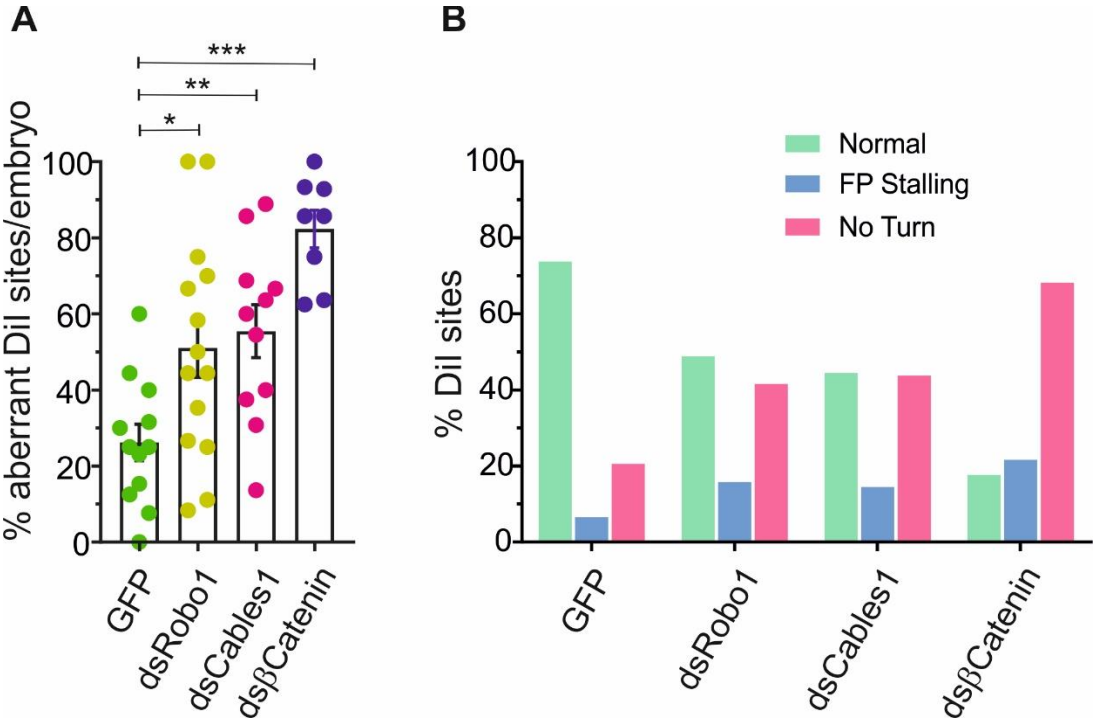

Fig. S5. The dsRNAs derived from *Cables1*, *β-Catenin*, and *Robo1* efficiently perturbed axon guidance when used at regular concentration

Using the regular concentrations of dsRNA derived from Robo1, β-Catenin (300 ng/µl), or Cables1 (500 ng/µl) to silence target genes effectively interfered with commissural axon guidance, as demonstrated earlier (Philipp et al., 2012; Alther et al., 2016; Avilés and Stoeckli, 2016). Knockdown of Robo1 was done by injection and electroporation of dsRobo1 at HH17-18, that is at a time that is not resulting in a maximal effect, as most Robo1 protein is made before that stage and stored in vesicles before being inserted into the growth cone surface by specific trafficking (Alther et al., 2016). However, we wanted to use the same protocol for all groups. Axonal trajectories were aberrant at 51.1±7.8% of the DiI sites in dsRobo1-treated embryos (n=143, N=14), at 55.5±7.0% of the DiI injection sites after silencing Cables1 (n=123 injection sites in N=11 embryos), and at 82.3±4.9% of the injection sites after silencing β-Catenin (n=91, N=8). Embryos injected with the plasmid encoding GFP were used as controls (same group as the one shown in Figure 6). Pathfinding was affected only at 26.2±4.8% of the injection sites in control-treated embryos (n=125 injection sites in N=12 embryos). *p=0.0207, **p=0.0094, ****p<0.0001 ANOVA with Tukey's multiple-comparisons test. (B) Looking at the individual phenotypes indicated that axons were both stalling more often and failed to turn at the exit site in experimental compared to control embryos.

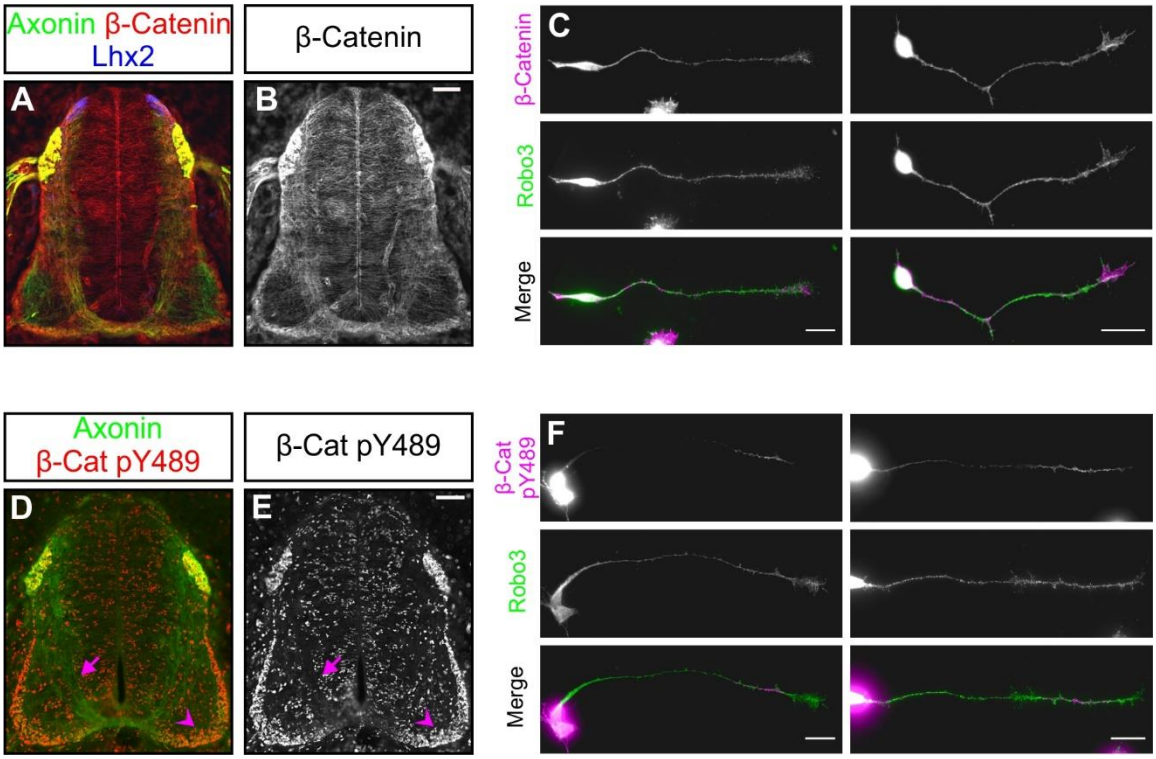

Fig. S6. A phosphorylated form of β-Catenin, β-Catenin pY489, accumulates in distal post-crossing axons

Transverse sections of spinal cords from HH26 embryos (A, B, D ,E) or dissected neurons (C, F) were stained for total β-Catenin (A, B, C) or β-Catenin pY489 (D, E, F). With an antibody recognizing all forms of β-Catenin, pre- and post-crossing axons were stained (A, B). In contrast, an antibody specific for β-Catenin that is phosphorylated at Y489 revealed higher levels of -β-Catenin pY489 on post-crossing axons (arrowhead), very low levels or no β-Catenin pY489 was found on pre-crossing axons (arrows) (D, E). Commissural axons and axons from dorsal root ganglia (DRG) neurons are visualized with an anti-Axonin1 antibody (green, A, D). Staining of cultures of dissociated neurons dissected from embryos sacrificed at HH26 demonstrates the accumulation of β-Catenin pY489 in the distal axon (F), whereas levels of total β-Catenin are more homogenous along the axon (C). Robo3, a marker for dI1 commissural axons is distributed equally along the axon (C, F). Scale bar: 50 µm in A,B,D,E; 20 µm in C,F.

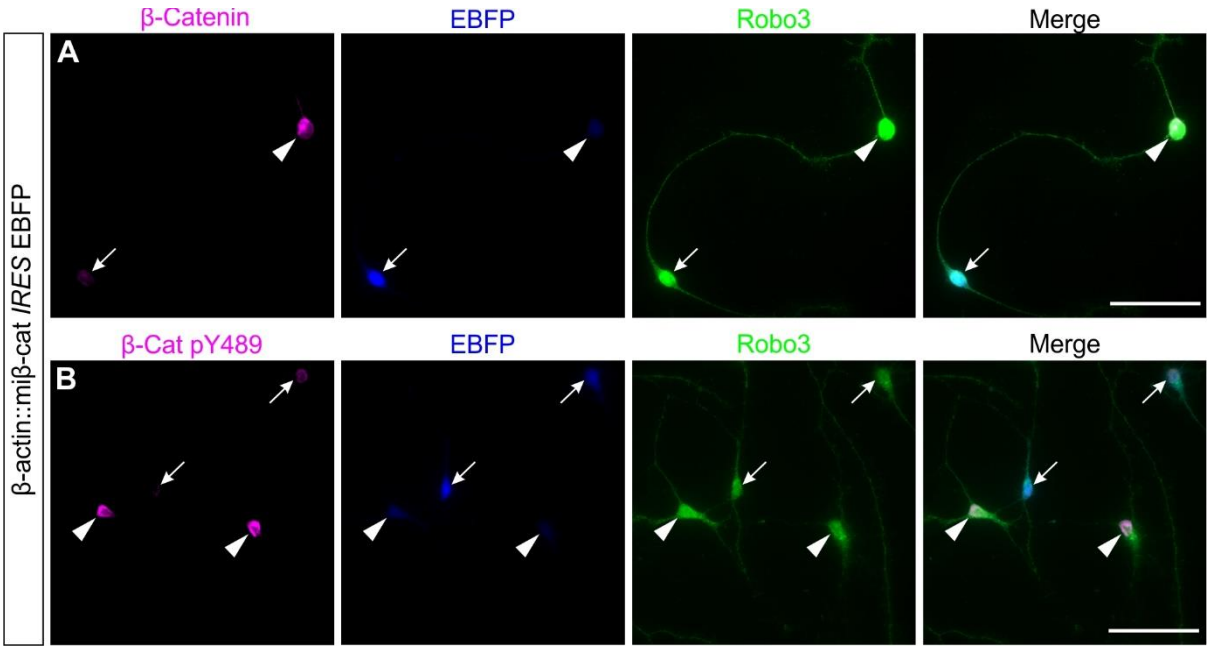

Fig. S7. Loss of β-Catenin in dI1 neurons can be visualized by staining with antibodies recognizing either β-Catenin or β-Catenin pY489.

To verify specificity of our approach and staining of either β-Catenin or β-Catenin pY489 we used a construct expressing a short-hairpin directed against β-Catenin followed by an IRES and blue-fluorescent protein (EBFP). After electroporation at E3, embryos were sacrificed two days later, at HH26, and dI1 neurons were isolated and kept in vitro for 2 days before fixation and staining. Panel A demonstrates that dI1 neurons (green, identified by their expression of Robo3) expressed β-Catenin (magenta; arrowhead). However, those cells that were efficiently targeted by electroporation (indicated by expression of EBFP; arrow) did not exhibit any β-Catenin staining. Similarly, using the monoclonal antibody specific for β-Catenin pY489 (magenta) revealed staining in Robo3-positive dI1 neurons (green) only, if they were not efficiently targeted by the plasmid (arrowhead; compare magenta staining in panel B with blue staining). Those that were efficiently targeted (arrows) did not show any β-Catenin pY489 staining. Bar: 50 µm.

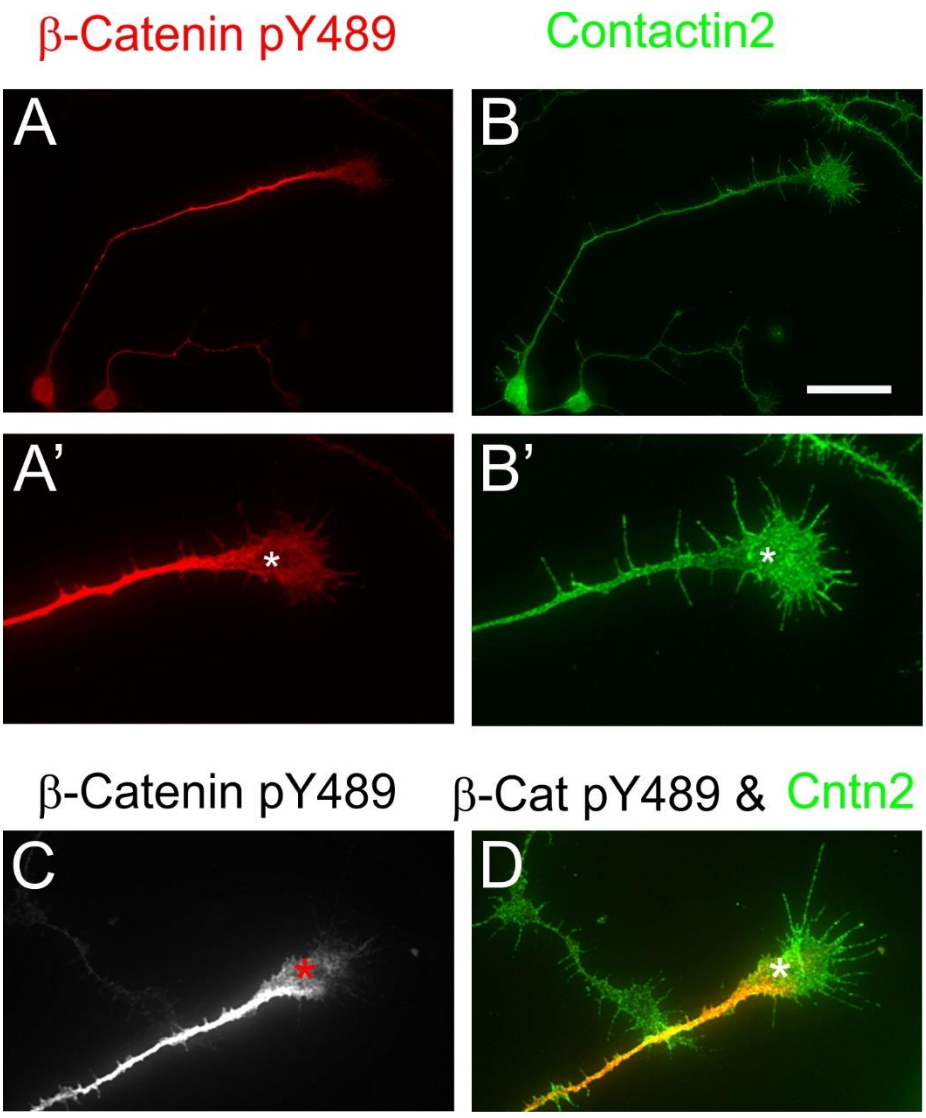

Fig. S8. β-Catenin pY489 localizes predominantly to the distal axon, the transition zone to the growth cone and in the central part of the growth cone.

In cultured post-crossing commissural axons, β-Catenin pY489 was found at higher levels in the distal axon (A; see also Figures 7 and 8). Contactin2 was used to stain axons and growth cones of dI1 neurons (B). β-Catenin pY489 is localized in the central part of the growth cone (A'), but not found in filopodia (compare staining for Contactin2 in B'). (C,D) Another example of a growth cone stained for β-Catenin pY489 (C) and shown in combination with Contactin2 staining (D, β-Catenin pY489 in red, Contactin2 in green). Bar: 20 µm in A,B; 10 µm in A',B',C,D.

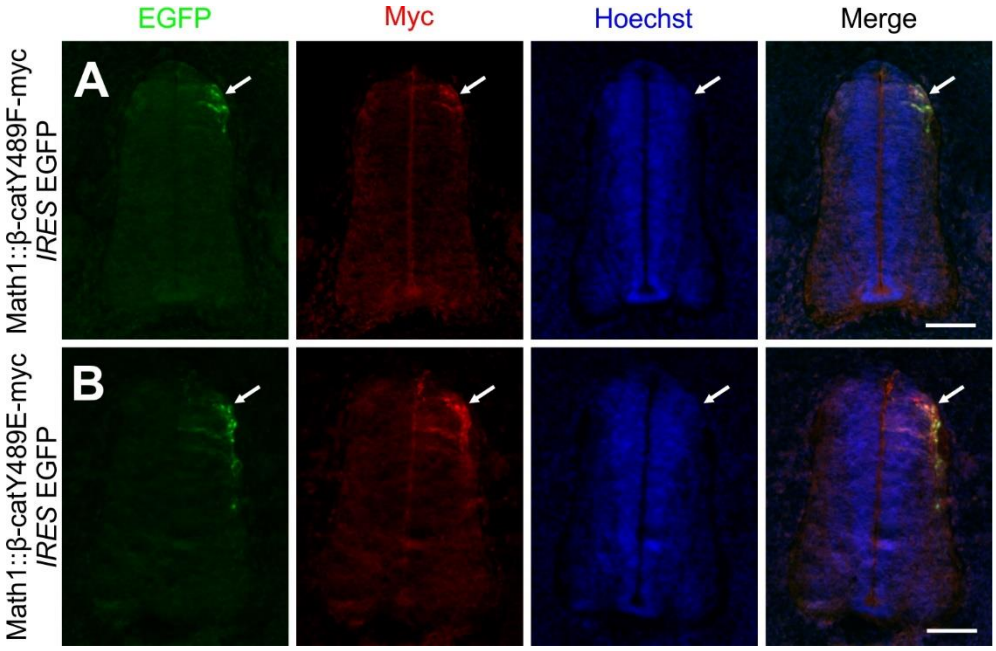

Fig. S9. Math1 drives expression of mutant version of β-Catenin.

Both the dominant negative version of β-Catenin, β-Catenin Y489F (A), which cannot be phosphorylated, and the dominant active version of β-Catenin, β-Catenin Y489E (B), are expressed in dI1 neurons when controlled by the Math1 enhancer. Electroporated constructs contained the myc-tagged version of the respective β-Catenin (either Y489F or Y489E) followed by an IRES site and EGFP. Hoechst staining shows nuclei.

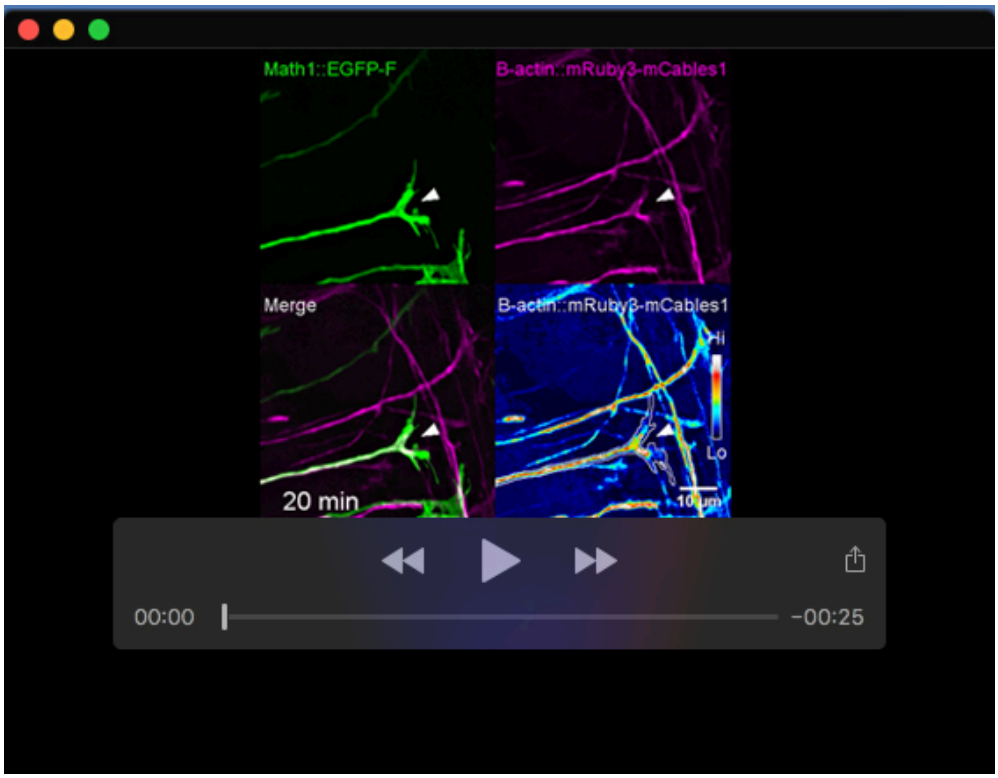

Movie 1. mRuby3-mCables1 localizes to dI1 growth cones at the floor-plate exit site.

Mouse Cables1 (mCables1) was fused to mRuby3 (shown in magenta) and electroporated *in ovo* into commissural neurons together with a Math1::EGFP-F plasmid to specifically label dI1 neurons (shown in green). This video shows a dI1 growth cone exiting the floor plate and turning rostrally (white arrowhead) in an intact cultured spinal cord using live imaging (see Figue 3A). In the lower right panel a heat map of pseudo-colored mRuby3-mCables together with the edge of the growth cone traced as a white line are shown. A clear signal of mRuby3-mCables could be seen in this growth cone during the exit of the floor plate as well as the rostral turn (white arrowhead). One stack was taken every 10 min for 90 min. Hi, high; Lo, low. Rostral is up.

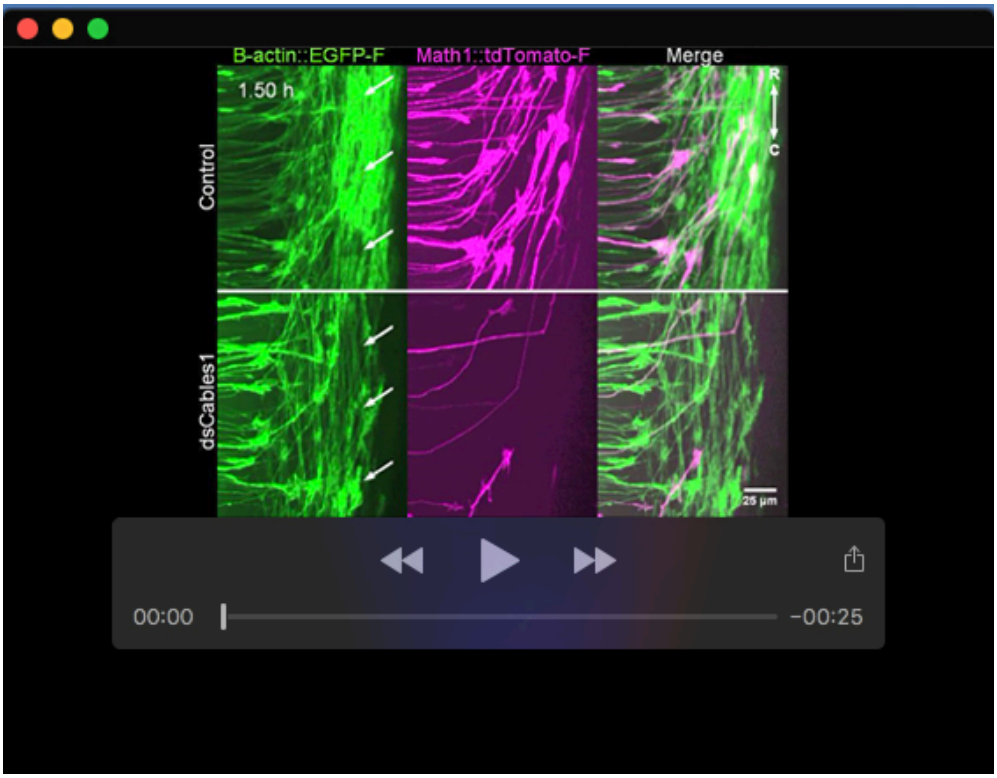

Movie 2. Twenty-four-hour time-lapse recording of dI1 axons crossing the floor plate in cultured intact spinal cords.

dI1 neurons were visualized by *in ovo* electroporation of the Math1::tdTomato-F plasmid (shown in magenta). In the control condition, dI1 axons turned rostrally in a well-organized manner after exiting the floor plate. However, knockdown of Cables1 induced aberrant phenotypes at the floor-plate exit site with axons turning caudally (yellow arrow) or having problems to extend rostrally (yellow arrowhead). These aberrant phenotypes clearly induced the formation of a disorganized ventral axon bundle as shown by all commissural axons expressing EGFP-F (green) compared to the tightly organized control funiculus (white arrows). R, rostral; C, caudal.